NASA/TM—2001–211383

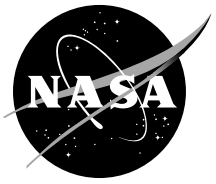

Absorbed Dose Determination Using Experimental and Analytical Predictions of X-Ray Spectra

D.L. Edwards
Marshall Space Flight Center, Marshall Space Flight Center, Alabama

November 2001

The NASA STI Program Office…in Profile

Since its founding, NASA has been dedicated to the advancement of aeronautics and space science. The NASA Scientific and Technical Information (STI) Program Office plays a key part in helping NASA maintain this important role.

The NASA STI Program Office is operated by Langley Research Center, the lead center for NASA's scientific and technical information. The NASA STI Program Office provides access to the NASA STI Database, the largest collection of aeronautical and space science STI in the world. The Program Office is also NASA's institutional mechanism for disseminating the results of its research and development activities. These results are published by NASA in the NASA STI Report Series, which includes the following report types:

- TECHNICAL PUBLICATION. Reports of completed research or a major significant phase of research that present the results of NASA programs and include extensive data or theoretical analysis. Includes compilations of significant scientific and technical data and information deemed to be of continuing reference value. NASA's counterpart of peer-reviewed formal professional papers but has less stringent limitations on manuscript length and extent of graphic presentations.

- TECHNICAL MEMORANDUM. Scientific and technical findings that are preliminary or of specialized interest, e.g., quick release reports, working papers, and bibliographies that contain minimal annotation. Does not contain extensive analysis.

- CONTRACTOR REPORT. Scientific and technical findings by NASA-sponsored contractors and grantees.

- CONFERENCE PUBLICATION. Collected papers from scientific and technical conferences, symposia, seminars, or other meetings sponsored or cosponsored by NASA.

- SPECIAL PUBLICATION. Scientific, technical, or historical information from NASA programs, projects, and mission, often concerned with subjects having substantial public interest.

- TECHNICAL TRANSLATION. English-language translations of foreign scientific and technical material pertinent to NASA's mission.

Specialized services that complement the STI Program Office's diverse offerings include creating custom thesauri, building customized databases, organizing and publishing research results…even providing videos.

For more information about the NASA STI Program Office, see the following:

- Access the NASA STI Program Home Page at ***http://www.sti.nasa.gov***

- E-mail your question via the Internet to help@sti.nasa.gov

- Fax your question to the NASA Access Help Desk at (301) 621–0134

- Telephone the NASA Access Help Desk at (301) 621–0390

- Write to:
  NASA Access Help Desk
  NASA Center for AeroSpace Information
  7121 Standard Drive
  Hanover, MD 21076–1320

NASA/TM—2001–211383

Absorbed Dose Determination Using Experimental and Analytical Predictions of X-Ray Spectra

D.L. Edwards
Marshall Space Flight Center, Marshall Space Flight Center, Alabama

National Aeronautics and
Space Administration

Marshall Space Flight Center • MSFC, Alabama 35812

November 2001

TRADEMARKS

Trade names and trademarks are used in this report for identification only. This usage does not constitute an official endorsement, either expressed or implied, by the National Aeronautics and Space Administration.

Available from:

NASA Center for AeroSpace Information
7121 Standard Drive
Hanover, MD 21076–1320
(301) 621–0390

National Technical Information Service
5285 Port Royal Road
Springfield, VA 22161
(703) 487–4650

TABLE OF CONTENTS

LIST OF FIGURES

LIST OF FIGURES (Continued)

LIST OF FIGURES (Continued)

LIST OF TABLES

LIST OF ACRONYMS AND SYMBOLS

BCI	beam current integration
CSDA	continuous slowing down approximation
EMU	extravehicular mobility unit
EVA	extravehicular activity
Fe	iron
FWHM	full width half maximum
H	hydrogen
$\dot{H}$	free radical for hydrogen
H_2O	water
H_2O_2	hydrogen peroxide
ISS	*International Space Station*
ISWE	international space welding experiment
ITS3	Integrated Tiger Series 3 (software package)
Li	lithium
MCA	multichannel analyzer
mGy	milli gray
MSFC	Marshall Space Flight Center
NASA	National Aeronautics and Space Administration
NIST	National Institute of Standards and Technology
NRC	Nuclear Regulatory Commission
OH	hydroxyl
$O\dot{H}$	free radical for hydroxel
PWI	Paton Welding Institute
rad	Roentgen absorbed dose
RBE	relative biological effectiveness
rem	unit of measure for tissue-equivalent absorbed dose
Si	silicon
Sv	sievert (new unit of dose equivalent)

LIST OF ACRONYMS AND SYMBOLS (Continued)

TLD	thermoluminescence dosimeter
TM	Technical Memorandum
TMG	thermal micrometeoroid garmet
UV	ultraviolet

NOMENCLATURE

A	atomic mass of the target material
a	factor that varies very slightly with atomic number
B_c	impact parameter
C	proportionality factor
C_1	conversion factor
C_E	conversion factor from x-ray intensity to x-ray flux
C_f	correction factor
C_{QE}	correction function for the SiLi quantum efficiency
c	speed of light in a vacuum
D	total absorbed dose rate in rem per hour
$D(E)$	dose rate at a specific x-ray energy
$(dE/dx)_{\text{col}}$	energy loss per unit pathlength
$(dE/dx)_e$	energy loss per unit pathlength due to interactions with bound electrons
$(dE/dx)_n$	energy loss per unit pathlength due to interactions with nucleus
$(dE/dx)_{\text{rad}}$	radiative stopping power
$(dE/dx)_T$	total energy loss per unit pathlength
$dI_{0\lambda}/dt$	number of x rays at wavelength λ per unit time
dx	infinitesimal thickness
$d\sigma/dk$	differential bremsstrahlung cross section
$d\sigma_e/dk$	bremsstrahlung cross section in the field of the atomic electrons
$d\sigma_n/dk$	bremsstrahlung cross section in the field of the screened atomic nucleus
E	energy
E_0	incident electron energy
E_E	x-ray energy at a specific energy
E_h	upper bound on the energy bin
E_l	lower bound on the energy bin
E_q	critical excitation energy
e	electron charge
f	$(1 + C\xi)^{-2}$
f_a	absorbed dose factor
$F(\tau)$	function

NOMENCLATURE (Continued)

$f_{T\phi}(E)$	total x-ray spectrum
$f_{\phi}(E)$	emitted bremsstrahlung spectral and intensity distribution at the surface of the impact target
h	number of electrons in the conduction band
I	mean excitation energy of the target material
I_0	monoenergetic x rays of intensity
$I_0(E)$	number of x rays of wavelength λ incident
$I_{0\lambda}$	bremsstrahlung spectrum
$I_{C\lambda}$	characteristic line intensity
$I(E)$	x-ray distribution
I_E	energy flux
I_{ITS3}	number of x rays per incident electron in a specific energy bin from software code ITS3
$I_{\mathrm{ITS3\text{-}C}}$	output from software code ITS3 in units of characteristic x rays per incident electron
$I_{\beta}(E)$	x-ray flux incident on the first layer of aluminized Mylar
K	empirical constant $\approx 1.3 \times 10^{-9}$
K_E	constant
$K_{\alpha 2}$	quantum of energy
k	energy of the emitted photon
k-factor	ratio of the tissue dose equivalent divided by mR*
k/T_1	ratio of the emitted photon energy divided by the kinetic energy of the interacting electron
L	inner shell electron
L_{II}	quantum states
M	inner shell electron
mc^2	electron kinetic energy unit
m_0c^2	electron rest mass energy
mR*	dose equivalent parameter
mSv	tissue dose equivalent
N	number of continuum photons
N_a	Avagadro's number
N_e	number of incident electrons per second interacting with the target
N_{e0}	number of electrons incident on the impact target
N_eT	total number of incident electrons impacting the target
n	number of electrons per gram mass in the absorber

NOMENCLATURE (Continued)

P_e	power imparted to a target by the incident electrons
p	final electron kinetic energy term = $[T\,(T + 2)]^{1/2}$
p_0	initial electron kinetic energy term = $[T_0(T_0 + 2)]^{1/2}$
P_x	power of emitted x rays
Q	quality factor
r_0	classical electron radius given by 2.82×10^{-14} mm
r_e	classical electron radius
T	final kinetic energy of an electron involved in a collision
T_0	initial kinetic energy of an electron involved in a collision
T_1	kinetic energy of the interacting electron
t	time
V	electron accelerating potential in volts
v	electron velocity
W_k	amount of energy required to remove an electron from the K shell
x	thickness
Z	target material atomic number
z	atomic number of incident particle
α	fine structure constant
β	electron velocity/c
γ	$1 / (1 - \beta^2)^{1/2}$
δ	x-ray production efficiency/density effect correction for the target material
η	cross section ratio
η_B	ratio of energy loss cross sections
λ	wavelength
λ_0	corresponding wavelength of E_0
λ_q	corresponding wavelength of E_q
μ	linear attenuation coefficient
$\mu(E)$	linear attenuation coefficient for the shielding material
$\mu(E)_1/\rho_1$	tabulated mass attenuation coefficient of the known material
$\mu(E)_x$	nontabulated linear attenuation coefficient of the desired material
μ_m	mass absorption coefficient
$\mu_{m\rho}$	linear attenuation coefficient
μ_t	mass absorption coefficient of the target

NOMENCLATURE (Continued)

μ_a	linear absorption coefficient
$(\mu_a/\rho)(E)$	mass energy absorption coefficient at a given energy
$(\mu_a/\rho)_{\text{med}}$	mass absorption coefficient for the medium
$\mu_\beta(E)$	linear attenuation coefficient for borosilicate
μ/ρ	mass attenuation coefficient
ξ	x-ray production efficiency $\left(\frac{1}{\lambda_0}^{1.65} - \frac{1}{\lambda_q}^{1.65}\right)\mu$, cosec ψ
ρ	density
ρ_x	density of the desired material
σ	x-ray scattering cross section
$\sigma_{ca}(E)$	energy absorption cross section for the Compton effect in barns/electron
σ_n	mass absorption coefficient
$\sigma_{pE}(E)$	photon cross section for photoelectric effect in barns/atom
$\sigma_{pp}(E)$	photon cross section for pair production in barns/atom
τ	kinetic energy of the interacting electron
Φ	photon emission intensity
ϕ_{rad}	dimensionless integrated bremsstrahlung energy loss cross section
$\phi_{\text{rad}(e)}$	energy loss cross section of a single electron
$\phi_{\text{rad}(n)}$	energy loss cross section in the field of the screened atomic nucleus
χ	μ_t cosec ψ
ψ	x-ray takeoff angle
Ω	solid angle of the SiLi detector
ω	frequency

TECHNICAL MEMORANDUM

ABSORBED DOSE DETERMINATION USING EXPERIMENTAL AND ANALYTICAL PREDICTIONS OF X-RAY SPECTRA

1. INTRODUCTION

The ability to join structures in space is recognized by the National Aeronautics and Space Administration (NASA) as a necessity. Near-term projects, for example, the *International Space Station* (*ISS*), will utilize joining techniques to assemble the structure in space. Future projects are investigating the possibility of using various joining technologies to assemble spacecraft and extraterrestrial bases. One of the joining techniques under consideration is electron beam welding. NASA has several concerns associated with electron beam welding in space and is working to resolve these issues. Issues such as accidental electron beam interaction with the astronauts' space suit, intensity of light generated by the electron beam welding process, and x-ray exposure to the astronaut as a result of performing electron beam welds are presently being investigated by NASA. This investigation focused on the x-ray exposure to astronauts performing electron beam welding in the vacuum of space.

NASA, in a joint venture with the Russian Space Agency, was scheduled to perform a series of welding in space experiments on board the U.S. Space Shuttle. This series of experiments was named the international space welding experiment (ISWE). This joint venture experiment was indefinitely delayed due, in part, to the rapidly degrading condition of the Soviet Space Station *Mir*.

The primary hardware item scheduled to be operated during this joint venture experiment was the ISWE handheld electron beam welding tool with a remote power supply. A Ukrainian company, the Paton Welding Institute (PWI), owns and operates the electron beam welding system. The ISWE electron beam welding hardware allows astronauts to perform welds in the vacuum of space. The ISWE electron beam welding tool produces an intense electron beam that deposits sufficient energy into the weld metal to join 6.4-mm (0.25-in.) structures. The ISWE electron source produces an electron beam of energy 8 keV and the electron beam current is variable from 52 to 76 mA. The interaction of this intense electron beam with the weld metal produces low-energy x rays (≤8 keV). The acronym ISWE will be applied to denote ground tests and space operations that utilize the PWI electron beam welding tool.

Manmade devices that emit radiation require confirmation that these radiations will not exceed the radiation dose to the astronaut, according to the Nuclear Regulatory Commission (NRC) limits for radiation workers.[1] The NRC radiation dose limits applicable for this effort are 18.75 rem per quarter for hands and forearms and 7.5 rem per quarter for the skin of the whole body.[2]

The protocol or summary issued by the PWI stated that the x-ray dose intensity produced by the operation of the ISWE electron beam source was measured to be 3.5 millirem/1,800 sec (3.5 millirem/30 min).[3] The ISWE was producing a 52-mA electron beam at 8 keV. The electron impact target was stainless steel. The results of this investigation indicate that the x-ray dosage value of 3.5 millirem/1,800 sec as presented by PWI is not correct. Dose intensity values will be presented in section 5 for various shielding configurations representative of the astronauts' protective space suit. The doses measured and calculated in this investigation are several orders of magnitude higher than the dose values presented by the protocol issued by PWI.

A series of ground-based experimental tests using the ISWE electron beam welding tool as the electron source and shielded thermoluminescence dosimeters (TLD's) as radiation detectors were performed. These tests indicated that an astronaut wearing a standard extravehicular activity (EVA) space suit would receive ≈8 rem to the forearm and shoulder while performing an 1,800-sec weld on aluminum. A flight operation schedule for the ISWE joint venture experiment indicates the astronaut would operate the ISWE electron beam welding tool for at least 3,600 sec (1 hr). This operation schedule would consist of at least one 1,800-sec ground-based training session using the ISWE hardware and one 1,800-sec welding operation during EVA on board the Space Shuttle. Under the existing flight operation schedule for the ISWE joint venture experiment, an astronaut could receive a dose of ≈16 rem in one calendar quarter. A dose of 16 rem was perceived as excessive for safe operation of the ISWE electron beam welding tool, since the maximum allowable dose is 18 rem per quarter.[1] An investigation was initiated to qualify additional radiation shielding material for the astronaut. One goal of the investigation was to reduce the astronauts' radiation exposure level to ≈2 rem per 1,800-sec ISWE operation. The ISWE operating parameters for the goal of 2 rem per 1,800 sec were defined as an electron energy of 8 keV, an electron beam current of 76 mA, and aluminum as the weld metal.

The ISWE hardware was returned to PWI before all issues pertaining to astronaut shielding could be resolved. Believing that NASA will one day utilize this electron beam welding in space technology, permission was granted to complete the investigation into x-ray shielding. With the ISWE hardware out of the country, an alternative method was needed to determine the radiation dose an astronaut would receive during operation of the ISWE electron beam welding tool. An analytical method was developed to calculate the absorbed dose using predicted x-ray spectral and intensity distributions produced during 8-keV electron interaction with metal.

Calculation of the x-ray spectrum begins with determining the production efficiency of x rays when energetic electrons interact with metal. Once the x-ray spectral and intensity distributions are determined, the x rays must be analytically propagated through x-ray-absorbing materials. Knowing x-ray attenuation coefficients for the absorbing materials allows calculation of the x-ray spectrum transmitted through the absorbing medium. The analytical method then uses this transmitted x-ray spectrum to calculate the absorbed radiation dose in the body.

This analytical approach was normalized to represent the electron beam intensity produced by the ISWE electron beam welding tool. This normalization allowed the calculated dose values to be compared with the dosage measured during the ISWE TLD exposure.

An experimental test system was developed to accurately reproduce the electron beam energy and x-ray flux produced by the ISWE electron beam welding tool. This test system used an electron

flood gun that produced an electron beam current orders of magnitude lower than the ISWE electron source. The test system possessed the capability to characterize the incident electron beam and the x rays that were generated by the electron-metal interaction. Characterization methodology consisted of a Faraday cup to measure the electron beam intensity and a Silicon Lithium-drifted (SiLi) detector to accumulate the x-ray spectrum. This test system experimentally accumulated x-ray spectral and intensity data. These data were used to verify the results of the analytical method that was used to calculate the x-ray spectrum. Utilization of both the experimental and analytical methods provides investigators with a tool that can be used to screen numerous candidate shielding materials.

This investigation developed analytical and experimental methods to calculate the absorbed dose in the body using x-ray spectra. The calculated absorbed dose values from x-ray spectra were normalized to an equivalent ISWE exposure. The calculated dose values were then compared to the dose values obtained from TLD's exposed during an 1,800-sec operation of the ISWE electron source. Calculated dose values were in good agreement with TLD measurements.

2. THEORY

The production of x rays by electron beam interaction with matter has been well documented by numerous authors for over 60 yr.[4–6] The x-ray production efficiency (ζ) from electron-impact sources is given by the following empirical relationship:[4,6]

$$\zeta = KZV \ , \tag{1}$$

where K is an empirical constant on the order of 1.3×10^{-9}, Z is the target material atomic number, and V is the electron accelerating potential in volts.[6]

This empirical relationship can be used to calculate the total energy of x rays produced, provided the incident electron energy and the Z of the target are known.[7] A more definitive approach is required to analytically determine the x-ray spectral and intensity distributions from electron impact targets.

Lindhard et al. published a series of papers on atomic collisions[8–10] that describes in detail the interaction of energetic ions with matter. A key factor in the approach of Lindhard et al. was to separate ion interaction with the target atom nucleus from the ion interaction with the bound electrons. Once this separation of interactions is recognized, calculations can be initiated to determine interaction-specific energy losses and cross sections. The energy loss, therefore, can be separated into two terms as:

$$(dE/dx)_T = (dE/dx)_n + (dE/dx)_e \ , \tag{2}$$

where the variable $(dE/dx)_T$ is the total energy loss per unit pathlength, $(dE/dx)_n$ is the energy loss per unit pathlength due to interaction with the nucleus, and $(dE/dx)_e$ is the energy loss per unit pathlength due to interactions with bound electrons.

Berger and Seltzer published a series of papers describing and calculating electron stopping powers, ranges, and bremsstrahlung generation.[11–14] Using the separation of interactions approach of Lindhard, Berger and Seltzer define the total electron stopping power as a sum of the collision stopping power and the radiative stopping power. Collision stopping power is the average energy loss per unit pathlength due to inelastic Coulomb collisions with bound atomic electrons in the target material. Collision interactions result in ionization and excitation of the target material. Radiative stopping power is the average energy loss per unit pathlength due to the emission of bremsstrahlung in the electric field of the atomic nucleus and the atomic electrons.[14] The separation of the electron stopping power into two components is useful for two reasons: (1) The methods used to evaluate the two components are different and (2) the energy going into the ionization and excitation of atoms is absorbed in the medium close to the initial electron penetration track. Most of the energy lost in the form of bremsstrahlung is absorbed far away from the initial electron penetration track. The total stopping power is given by[13,14]:

$$-(1/\rho)(dE/dx)_T = -(1/\rho)(dE/dx)_{\text{col}} - (1/\rho)(dE/dx)_{\text{rad}} \ . \tag{3}$$

The equation for the collision stopping power $(dE/dx)_{\text{col}}$ is given as[13,14]:

$$(dE/dx)_{\text{col}} = [(2\pi N_a r_e^2 mc^2 Z)/\beta^2 A] \{\log [\tau^2(\tau+2) / 2(I/mc^2)^2] + F(\tau) - \delta\} \ . \tag{4}$$

In equation (4), N_a is Avagadro's number, r_e is the classical electron radius, mc^2 is the electron rest mass energy (0.511 MeV), Z is the atomic number of the target material, τ is the kinetic energy of the interacting electron in units of mc^2, I is the mean excitation energy of the target material, β is defined as the electron velocity/c, A is the atomic mass of the target material, and δ is a density effect correction for the target material. The function $F(\tau)$ is defined as:

$$F(\tau) = 1 - \beta^2 + [\tau^2/8 - (2\tau+1)\log 2] / (\tau+1)^2 \ . \tag{5}$$

The equation for the radiative stopping power $(dE/dx)_{\text{rad}}$ is given by[14]:

$$(dE/dx)_{\text{rad}} = (N_a/A)\alpha r_e^2 Z^2 (T_1 + mc^2)\phi_{\text{rad}} \ , \tag{6}$$

where α is the fine structure constant, and T_1 is the kinetic energy of the interacting electron. The parameters N_a, A, r_e, Z, and mc^2 were previously defined. The parameter ϕ_{rad} is the dimensionless integrated bremsstrahlung energy loss cross section. The equation for ϕ_{rad} is given by[11]:

$$\phi_{\text{rad}} = \int_0^{T_1} k\,(d\sigma/dk)dk/[\alpha r_e^2 Z^2 (T_1+mc^2)] \ , \tag{7}$$

where $d\sigma/dk$ is the differential bremsstrahlung cross section, T_1 is the kinetic energy of the incident electron, and k is the energy of the emitted photon. Using the approach of Lindhard et al., the parameter ϕ_{rad} is expressed as the sum of two components:

$$\phi_{\text{rad}} = \phi_{\text{rad}(n)} + Z\phi_{\text{rad}(e)} \ . \tag{8}$$

The terms $\phi_{\text{rad}(n)}$ and $\phi_{\text{rad}(e)}$ are, respectively, the energy loss cross section in the field of the screened atomic nucleus and the energy loss cross section of a single electron. The ratio of these energy loss cross sections is presented in terms of the quantity:

$$\eta_B = \phi_{\text{rad}(e)}/[(1/Z^2)\ \phi_{\text{rad}(n)}] \ . \tag{9}$$

Values of η_B and ϕ_{rad} in equation (9) are tabulated in a paper by Berger and Seltzer[11] and can be used to calculate the fractional radiative energy loss due to electron-nucleus interactions and electron-electron interactions using:

$$\phi_{\text{rad}(n)} = (Z/(Z + \eta_B))\phi_{\text{rad}} \ , \tag{10}$$

and

$$\phi_{\text{rad}(e)} = [\eta_B /(Z(Z + \eta_B)]\phi_{\text{rad}} \ . \tag{11}$$

Bethe and Heitler[15] and Segrè[16] discuss the contribution to energy loss per unit pathlength from collision and radiative interactions. These authors state the ratio of the radiative loss to the collision loss can be approximated by:

$$(dE/dx)_{\text{rad}} / (dE/dx)_{\text{col}} \approx EZ/1{,}600\ mc^2 \ . \tag{12}$$

Considering the case of 8-keV electrons incident on aluminum and using equation (12), the collision process dominating the energy loss process is easily determined. This simple calculation indicates that the collision interaction is important and in fact dominates the energy loss process in the energy range of interest to this investigation. The focus of this investigation was to analytically predict the bremsstrahlung spectrum generated by electron impact sources. Therefore, the concentration will be on the radiative contributions and not on the collision contributions to bremsstrahlung cross sections. As a final note on the collision process, this process must be continuously monitored during the electron penetration of the target. Accurate monitoring of this collision energy loss is required to accurately determine the total energy loss, as described in equation (3).

Berger and Seltzer[11,12] define the bremsstrahlung cross section ($d\sigma/dk$) as the sum of two terms:

$$d\sigma/dk = (d\sigma_n/dk) + Z(d\sigma_e/dk) \ . \tag{13}$$

In equation (13), the term ($d\sigma_n/dk$) represents the bremsstrahlung produced in the field of the screened atomic nucleus. The term $Z(d\sigma_e/dk)$ represents the bremsstrahlung produced in the field of the Z atomic electrons. Berger and Seltzer[11] define the cross-section ratio of electron-nucleus bremsstrahlung and electron-electron bremsstrahlung as:

$$\eta = d\sigma_e/dk \ / \ [(1/Z^2)(d\sigma_n/dk)] \ . \tag{14}$$

The two components of the bremsstrahlung cross section can be extracted from equation (14) by using the relationships:

$$d\sigma_n/dk = (Z/(Z + \eta))d\sigma/dk \ , \tag{15}$$

and

$$d\sigma_e/dk = (\eta/(Z + \eta))d\sigma/dk \ . \tag{16}$$

Tabulated values of η, η_B, $d\sigma/dk$, and ϕ_{rad} are presented by Berger and Seltzer[11] which allow calculation of $d\sigma_n/dk$, $d\sigma_e/dk$, and $(dE/dx)_{\text{rad}}$ for specific values of T_1 and k/T_1, where T_1 is the kinetic energy of the interacting electron and k/T_1 is the ratio of the emitted photon energy divided by the kinetic energy of the interacting electron.

Halbleib et al.[17] utilized the results of Berger and Seltzer[11] to generate the software package Integrated Tiger Series 3 (ITS3). The data tabulated by Berger and Seltzer contain bremsstrahlung cross-section information and cross-section ratio information for specific energies between 1 keV and 10 GeV. Berger and Seltzer evaluated the bremsstrahlung cross sections for fixed values of k/T_1. ITS3 was used in the analytical work in this investigation to calculate the bremsstrahlung spectrum from electron

impact on various targets. ITS3 uses a cubic spline interpolation among the data, by Berger and Seltzer, to evaluate the cross section for desired values of T_1 and k/T_1, where T_1 is the energy of the interacting electron and k is the energy of the emitted photon. Once the values of the bremsstrahlung cross sections are obtained, the ITS3 software package calculates the number of photons of energy k emitted for a specific cross section. ITS3 includes a self-absorbing calculation for photons originating at depth within the target. This self-absorption calculation accounts for Compton scattering and photoelectric effect interactions.

Photoelectric effect absorption is the dominant interaction for the x-ray energy range of this investigation.[6] Embedded in the calculations for photoelectric absorption is the Auger effect photon absorption process. The Auger effect is the process by which an atom fills an inner shell electron vacancy with an electron from a higher shell and releases the energy of the transition by electron emission. The Auger effect is more common in elements of low atomic number because the electrons are more loosely bound and the photons are more readily absorbed.[18]

Sulkanen[19] uses the Koch and Motz[20] bremsstrahlung cross section for unscreened atomic nuclei and the electron energy loss equation given by Jackson[21] and applied a continuous slowing down approximation (CSDA) in his software code XG.[22]

The Koch and Motz equation for the unscreened, nonrelativistic electron bremsstrahlung cross section is given by:

$$d\sigma/dk = (Z^2 r_0{}^2/137)(16/3kp_0{}^2)[\ln(p_0 + p)/(p_0 - p)] \quad . \tag{17}$$

In equation (17), Z is the target atomic number, r_0 is the classical electron radius given by (2.82×10^{-14} mm), and k is the energy of the emitted photon in $m_o c^2$ units. The terms p_0 and p in equation (17) are defined as:

$$p_0 = [T_0(T_0 + 2)]^{1/2} \quad , \tag{18}$$

and

$$p = [T(T + 2)]^{1/2} \quad , \tag{19}$$

where T_0 and T are the initial and final kinetic energies of an electron involved in a collision, respectively. The energy loss per unit pathlength given by Jackson[21] is:

$$dE/dx = 4\pi NZ(z^2 e^4/mv^2)[\ln(B_c - v^2/c^2] \quad , \tag{20}$$

where

$$B_c = (\gamma - 1)[(\gamma + 1)/2]^{1/2} \, (mc^2/h<\omega>) \quad , \tag{21}$$

and

$$\gamma = 1/(1 - \beta^2)^{1/2} \quad . \tag{22}$$

Sulkanen[19] shows comparison plots with the x-ray spectra generated by the XG software package, the results of Pella et al.,[23] and experimental data. The XG model is in good agreement with Pella's results and the experimental data. Sulkanen[19] shows that variations of approximately a factor of 2 exist over a wide range of x-ray energies, with larger discrepancies at lower x-ray energies. Sulkanen's results, for an incident electron of 8 keV, impinging an aluminum target, were found to be in good agreement with ITS3 and experimental data. A plot comparing the results of Sulkanen, the ITS3 model, and experimental data is shown in section 5, figure 12.

Pella et al.[23] developed a method to calculate the x-ray continuum produced by electron impact sources. Pella starts with an equation for the number of continuum photons in a unit energy interval (dE), given as:

$$N(E)dE = K_E Z[(E_0 - E)/E]dE \quad . \tag{23}$$

In equation (23), E is the energy of the continuum photon, E_0 is the incident electron energy, and K_E is a constant. If equation (23) is expressed in wavelength units, then K_E has a value of 2.76×10^{-6} and equation (23) can be written as:

$$N(\lambda) = 3.42 \times 10^{-5}\, Z(\lambda/\lambda_0 - 1)\lambda^2 \quad . \tag{24}$$

Rewriting equation (24) in terms of unit solid angle gives:

$$I(\lambda) = N(\lambda)/4\pi = 2.72 \times 10^{-6}\, Z(\lambda/(\lambda_0 - 1)\lambda^2 \quad . \tag{25}$$

Pella et al.[23] states "that other workers have used Monte Carlo methods to simulate the x-ray production within the x-ray tube target. These methods, however, require extensive computer capabilities. Because parameters, such as ionization cross section, target absorption factor, backscatter factor, and fluorescence yield are not known with sufficient accuracy, it is important to use measured x-ray output spectral distributions if a reliable algorithm is to be developed." Pella et al.[23] incorporates a proportionality factor (C) into his algorithm to account for these parameter inaccuracies. Introduction of this proportionality factor begins with Pella indicating that an accurate model for the calculation of the continuum distribution must include target self-absorption of photons and also the detector absorption characteristics. Pella makes the assumption that characteristic and continuum x rays have the same depth distributions, meaning that they have the same amount of absorption. The expression:

$$1/f = (1 + a\gamma\chi)^2 \quad , \tag{26}$$

is given to account for the self-absorption of photons in the target. In equation (26), a is a factor that varies very slightly with atomic number, χ is defined as $\mu_t \operatorname{cosec}\psi$, where μ_t is the mass absorption coefficient of the target and ψ is the x-ray takeoff angle.

The term γ in equation (26) is given by:

$$\gamma = (E_0^{1.65} - E_q^{1.65}) \quad , \tag{27}$$

where E_0 is the interacting electron energy and E_q is the critical excitation energy. Pella states that equation (27) is proportional to:

$$\gamma \propto (1/\lambda_0^{1.65} - 1/\lambda_q^{1.65}) \ , \tag{28}$$

where λ_0 and λ_q are the corresponding wavelengths of E_0 and E_q. Now, Pella defines the term ξ as:

$$\xi = (1/\lambda_0^{1.65} - 1/\lambda_q^{1.65})\ \mu_t \operatorname{cosec}\psi \ . \tag{29}$$

The proportionality factor (C) is introduced by expressing equation (26) as:

$$f = (1 + C\xi)^{-2} \ . \tag{30}$$

Pella et al.[23] state that the continuum intensity can now be expressed as:

$$I'(\lambda) = I(\lambda) f \ , \tag{31}$$

using an expression for C given by:

$$C = [1 + (1 + 2.56 \times 10^{-3}\ Z^2)^{-1}] \ / \ [(1 + 2.56 \times 10^3\ \lambda_0 Z^{-2})(0.25\xi + 1 \times 10^4) \ . \tag{32}$$

Pella et al.[23] show good agreement with experimental results but their model consistently underpredicts experimentally accumulated x-ray spectral intensity.

The units used to quantify absorbed doses of radiation and the tissue equivalent radiation doses have changed during the past years. The quantity of absorbed dose was officially adopted in 1953 to be defined as a rad, which is an acronym for Roentgen absorbed dose.

A rad is defined as 100 ergs of deposited energy per gram of material. The rad did not account for the differences in biological effects due to the different types of radiation; i.e., x rays, electrons, and neutrons, of various energies. To account for the relative biological effectiveness (RBE), a unit of measure for the tissue-equivalent absorbed dose was defined. This unit of equivalent dose was the rem. The conversion from rem to rad is given by:

$$1 \text{ rem} = 1 \text{ rad} \times Q \ , \tag{33}$$

where Q is defined as the quality factor and is a modifying factor by which the absorbed dose, in rads, can be multiplied to determine the risk of biological injury corresponding to the irradiation conditions.[24] The new unit of absorbed dose is the gray. The conversion from rads to gray is given by:

$$1 \text{ gray} = 100 \text{ rads} \ . \tag{34}$$

The unit of dose equivalent has also changed. The new unit of dose equivalent is the sievert (Sv). The conversion from absorbed dose in gray to the equivalent dose in sievert is given by:

$$\text{Sv} = \text{gray} \times Q \ , \tag{35}$$

i.e., 1 Sv equals 100 rem with Q equal to 1.

The conversion of photon flux, or photon energy, to absorbed dose was published as early as 1959 by Henderson.[25] Henderson states that the mass energy absorption coefficients for gamma rays can be calculated using:

$$[\mu_a/\rho](E) = [\sigma_{ca}(E)\ (0.6025)\ (z)]\ /(A) + [\sigma_{pp}(E)]C_1 + [\sigma_{pE}(E)]C_1\ . \tag{36}$$

In equation (36), $[\mu_a/\rho](E)$ is the mass energy absorption coefficient at a given energy (E) in cm^2/gm, $\sigma_{ca}(E)$ is the energy absorption cross section for the Compton effect in barns/electron, Z is the atomic number of the target material, A is the atomic weight of the target material, $\sigma_{pp}(E)$ is the photon cross section for pair production in barns/atom, $\sigma_{pE}(E)$ is the photon cross section for photoelectric effect in barns/atom, and C_1 is a conversion factor for each element such that barns/atoms = cm^2/gm. Dyson[6] states that the photoelectric effect is one of the most important interactions in the energy region of 1 to 100 keV.

Defining the photoelectric effect as the dominant interaction for low-energy photon interaction with matter, equation (36) reduces to:

$$[\mu_a/\rho](E) \approx [\sigma_{pE}(E)]C_1\ \ , \tag{37}$$

for the photon energy range considered in this investigation.

The photoelectric effect consists of x-ray absorption by a target electron and the subsequent removal of that bound electron from the atom in the target. In general, the inner shell electrons are the predominant contributors to the photoelectric effect. The inner shell electrons are denoted as the K, L, and M shell electrons. The photoelectric effect is subject to the overriding consideration that the incident photon energy must be greater than the binding energy of the electron bound to the target atom if photoelectric absorption is to occur. Photoelectric absorption occurs most readily if the binding energy is comparable with the incident photon energy. Henderson provides graphed data to determine the conversion factor C_1 in equations (36) and (37). Once C_1 is determined, the mass energy absorption coefficient can be calculated. More recent data, tabulated by Hubbell[26] and also found on the Internet,[27] were used to determine the value of the mass energy absorption coefficient. Henderson determines that:

$$1\ \text{MeV/cm}^2\text{/sec} = 5.76 \times 10^{-5}\ [\mu_a/\rho](E)\ \text{rads/hr}\ \ , \tag{38}$$

given the incident photon flux is represented by energy flux. This conversion from photon energy flux to absorbed dose is identical to the results of Fitzgerald et al.[28]

Schollhammer, while working for the Hamilton Standard division of United Aircraft Corporation, presented a document of x-ray dosimetry from electron beams utilized as a welding tool for commercial application.[29] The Hamilton Standard division of United Aircraft Corporation developed a handheld electron beam welding tool suitable for astronauts to operate on EVA. Schollhammer recognized the need for a multipurpose welding system and states that electron beam welding will satisfy this need. This electron beam welding system can operate at accelerating potentials as high as 20 kV with electron beam currents as high as 100 mA. Operating at these parameters, Schollhammer recognized the potential for a radiation exposure hazard. Schollhammer performed computations indicating that 7.87×10^{-3} mm

(0.031 in.) of steel would adequately attenuate 20 keV x-ray radiation to a safe level of <1 millirem/1,800 sec (1 millirem/30 min). Schollhammer included a radiation-vapor shield as part of the electron beam welding system. This radiation-vapor shield could be positioned so that it totally surrounds the electron-impact site or the shield could be removed entirely. The radiation-vapor shield was 1.02×10^{-3} mm (0.04 in.) thick and made of stainless steel. Schollhammer performed a series of tests with and without the radiation-vapor shield.

Schollhammer selected two types of radiation monitoring systems: A Victoreen model 440 radio frequency shielded radiation meter and photosensitive film badges. During the first test, the radiation-vapor shield was removed from the electron beam welding tool. A Victoreen model 440 radiation meter was positioned exterior to the vacuum system and the x rays were passed through a thin Mylar® window. Various absorbers were placed in front of the radiation meter to determine shielding effectiveness. This test concluded that 1.02×10^{-3} mm (0.04 in.) of steel was sufficient to attenuate the emitted radiation to a safe level of <1 millirem/1,800 sec.

The second test, conducted by Schollhammer, included the radiation-vapor shield surrounding the electron beam welding tool. Photosensitive film badges were positioned at various locations in the vacuum chamber around the weld target. The Victoreen model 440 radiation meter was positioned exterior to the vacuum chamber with radiation passing through the Mylar window. Tungsten was used as the weld target with the electron beam welding tool operating at 15 kV and 100 mA for 15, 30, and 45 sec. Schollhammer states that neither the Victoreen model 440 or the photosensitive film badges recorded any measurable radiation.

Information received from Kuhar[30] indicates that the sensitivity of the Victoreen model 440 may not be sufficient to accurately measure the x rays emitted by the operation of the Hamilton Standard electron beam welding tool. The energy range of the model 440 is 10 keV to 0.5 MeV, and the energy efficiency curve for this meter indicates 70-percent efficiency at 10 keV.[30] Schollhammer states that the photosensitive film badges are sensitive enough to register 1 millirem at 15 keV. The bremsstrahlung radiation, generated by this electron beam welding tool, is continuous with a maximum energy of 15 keV. The response of the film badge at energies lower than 15 keV was not stated. It is possible that the instrumentation used by Schollhammer lacks the sensitivity to detect low-energy x rays. The results of the paper by Schollhammer state that the measured radiation exposure agrees with calculated values.

PWI, a research agency of the Ukrainian government, provided a report, "Protocol of Testing the Universal Technological Hardware," detailing a radiation dosimetry test performed in 1984.[3] This document is a translated test report detailing the results of an experiment to determine the x-ray exposure to an EVA cosmonaut operating the ISWE electron beam weld tool. The protocol states that a stainless steel target was impacted by 8-keV electrons with an electron beam current of 52 mA. The exposure time was stated in the protocol as 18.708 sec. The x-ray detector reported to have been used in this investigation was a SiLi-drifted detector. The SiLi detector was positioned 700 mm from the target and 200 x-ray counts were recorded during the ISWE test. The results of this protocol state that 200 x-ray counts correspond to a radiation exposure environment of 3.5 millirem/1,800 sec.

Calculations described in section 6 and experimental data shown in section 5 show the values of 200 counts, and subsequently, 3.5 millirem/1,800 sec are not correct.

Harris and Edwards[31] published a paper in 1997 that describes the use of TLD's to measure radiation dose from low-energy x rays. The low-energy x rays were generated by an electron beam interacting with aluminum. The electron beam energy was 8 keV and the beam current was 76 mA. The TLD's were positioned in a vacuum chamber with the electron source. The TLD's were located 584 mm (23 in.) from the electron impact site and many of the TLD's were shielded by materials identical to those comprising the astronauts' space suit and helmet. The exposure time to the x-ray flux was 1,800 sec (30 min). Analysis of the TLD's indicated a measurable and higher than expected radiation dose. This Technical Memorandum (TM) is the first known application of TLD's to measure radiation dose from low-energy x rays. The results of this TM were used to verify dosimetry calculations in this investigation.

X rays are electromagnetic radiation of exactly the same nature as visible light, except that their wavelength is several orders of magnitude shorter. X rays travel in straight lines, are uncharged, exhibit wave motion phenomenon, and can be polarized. Customarily, x rays are defined as photons of wavelengths in the range of 10 to 0.1 Å that are produced artificially. The term gamma ray is reserved for the radiations emitted spontaneously by radioactive nuclei.[32]

It is well known that when electrons of sufficient energy interact with matter, x-rays are produced.[1,4,5,21,32] Roentgen is credited with this discovery and numerous investigators have utilized his discovery for applications too diverse to adequately cover in this TM.[4,33,34] Two general processes, characteristic x-ray emission and continuous x-ray emission or bremsstrahlung, dominate x ray production from electron impact sources. The essential condition for the production of a characteristic x ray is that an electron be removed from an inner shell of the target atom.

Using the Bohr model of the atom, the following description of the production of characteristic x rays is provided.[35] Suppose an inner shell electron, *K* shell electron, is ejected from an atom by the absorption of energy from an incident electron. The amount of energy required to remove an electron from the *K* shell is denoted as W_k. The atom is now said to be in the *K* quantum state. The resulting vacancy in the *K* shell can be filled by an outer shell electron, for example an *L* or *M* shell electron, "falling" into it. For this description, assume the *K* vacancy is filled by an L_{II} electron. Now the *K* shell is filled but the *L* shell has a vacancy. The atom is now said to be in the L_{II} quantum state. In going from the *K* state to the L_{II} state, the atom's energy has decreased, so the conservation of energy requires that a quantum of energy be given off.

This quantum of energy is referred to as $K_{\alpha 2}$ and is represented by the following equation:

$$K_{\alpha 2} = W_k - WL_{\mathrm{II}} \ , \tag{39}$$

where $K_{\alpha 2}$ is the energy of the characteristic x ray.

Continuous or bremsstrahlung x rays are produced when electrons lose energy in passing through the Coulomb field of a nucleus or bound electron. Consider an electron of initial energy E_0 moving in the Coulomb field of the target atom nucleus. The Coulomb field can cause the incident electron to change its direction of motion. According to classical concepts of charge acceleration, every change in direction involves an acceleration.[21] Therefore, it is probable that in passing a nucleus the electron will emit a quantum of energy (k) and will drop to a new state at energy E, where $E = E_0 - k$. The probability that a quantum of energy (k) will be emitted is dependent upon the bremsstrahlung cross section ($d\sigma/dk$).

The physical significance of the bremsstrahlung cross section can be expressed as the area or cross section that each nucleus, or bound electron, presents to the bombarding particle. For this investigation, the bombarding particle was an electron. The nucleus, in whose field the photon is emitted, is considerably heavier than the electron and it can acquire, in principle, any transfer of momentum ranging from zero to $m_0 v_0$.[36] In theory, the bremsstrahlung spectrum, due to electron-nucleus interactions, is continuous over the energy range from 0 to E_0.

Critical to this investigation is the accurate determination of the x-ray production efficiency from electron-impact targets. The simplest method used to calculate the x-ray production efficiency was given by equation (1). This empirical relationship was used to calculate the total number of x rays produced, given the incident electron energy and Z of the target.[7] A more definitive approach was needed for this investigation to analytically determine the bremsstrahlung spectral and intensity distribution. The author developed an analytical method to determine the x-ray spectral and intensity distribution from an electron-impact source. Verification of the analytical approach was achieved by comparing the analytical spectra with experimental spectra.

The following relationship was empirically derived by the author to calculate the x-ray spectrum that would be measured by an SiLi-drifted detector:

$$dI_{0\lambda}/dt = f_{\phi}(E)\Omega N_e C_{QE} \ . \tag{40}$$

The variable on the left-hand side of equation (40), $dI_{0\lambda}/dt$, is the number of x rays of wavelength λ per unit time incident on the detector. The right-hand side of equation (40) contains geometry-specific variables, where $f_{\phi}(E)$ is the emitted bremsstrahlung spectral and intensity distribution at the surface of the impact target, Ω is the solid angle of the SiLi detector, N_e is the number of incident electrons per second interacting with the target, and C_{QE} is the correction function for the SiLi quantum efficiency. Descriptions of each of the geometry-specific variables in equation (40) are discussed below.

The function $f_{\phi}(E)$ is the x-ray spectral and intensity distribution emitted from the surface of an electron impact target, obtained using ITS3. ITS3 is a software package designed for state-of-the-art Monte Carlo solution of linear time-independent coupled electron/photon radiation transport problems.[17] The form of the function $f_{\phi}(E)$ used in equation (40) requires manipulation of the data generated by the ITS3 software. A discussion of the ITS3 code and its use to determine the function $f_{\phi}(E)$ is described in section 3.

The constant Ω is the solid angle of the detector. This specific application utilizes the SiLi detector, positioned at a distance of 584 mm (23 in.) from the impact target. The solid angle for this specific geometry was 5.6×10^{-6} sr.

The variable N_e is the number of electrons incident on the impact target per second. The value of N_e was empirically determined using beam current integration (BCI) techniques. The value N_e is actually of the form:

$$N_e t = N_{e0}\,(C_f + 1) \ , \tag{41}$$

where N_{e0} is the total number of electrons incident on the impact target as measured by the BCI electronics, t is the time the electron beam was incident on the target, and C_f is a correction factor to account

for the secondary electron emission not counted by BCI. The correction factor (C_f) was empirically determined by comparing the electron beam current measured at the impact target to the electron beam current measured using a Faraday cup with a large aspect ratio. Many interactions occur as incident electrons impact the target. Incident electrons may penetrate deep in the target and eventually come to rest. This addition of one electron charge is "counted" by the BCI system. As this electron traverses deep into the flat plate target, it may ionize a target atom by removing bound electrons. These liberated electrons may escape the target and come to rest in the wall of the test chamber. The test chamber was electrically isolated from the target. This action effectively places a positive charge on the target which the BCI system records as a positive charge deposition event, thus canceling a negative deposition charge event. The utilization of a large aspect ratio Faraday cup allows collection of the liberated secondary electrons. The aspect ratio is the ratio of the length of the Faraday cup to the entrance diameter. A large aspect ratio provides a small solid angle for escape of emitted secondary electrons. Therefore, when a secondary electron is emitted from the surface, the BCI records a positive event due to the positively ionized target atom. The Faraday cup collects this emitted secondary electron which is recorded by the BCI system as a negative event. These positive and negative events, due to secondary electron emission, cancel. The net result to the BCI system of one electron is counted. Figures 1 and 2 detail the secondary electron emission geometry of a Faraday cup and a flat plate.

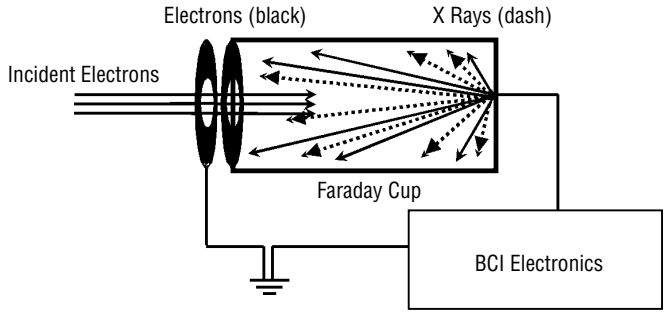

Figure 1. Secondary electron emission geometry inside a Faraday cup.

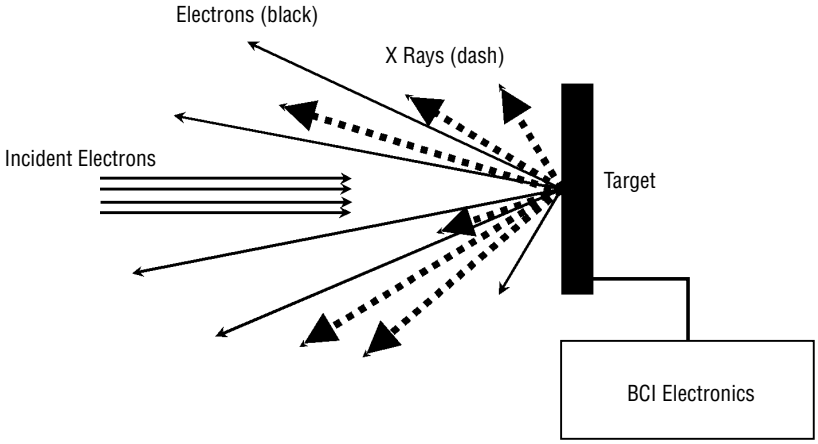

Figure 2. Secondary electron emission geometry originating from a flat plate.

The term C_{QE} in equation (40) is a correction function to account for the quantum efficiency of the SiLi detector. This function is dependent on the x-ray energy. The quantum efficiency curve was provided by the SiLi manufacturer and is shown in figure 3.[37] Quantum efficiency data, obtained from the curve in figure 3, were extracted from a plot provided by Canberra, the manufacturer of the SiLi detector. Using this quantum efficiency data, the author determined a set of equations relating the SiLi quantum efficiency as a function of x-ray energy. This set of equations covers the x-ray energy range applicable for this investigation.

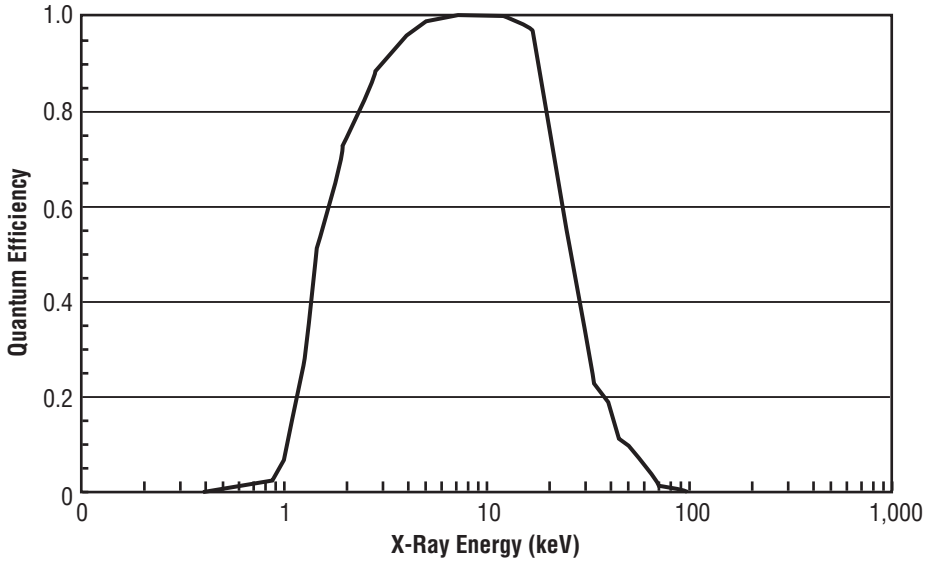

Figure 3. Quantum efficiency curve for the SiLi detector used in this investigation.

Over the x-ray energy range of 1 to 15 keV, the quantum efficiency can be described by the following relation:

$$C_{QE} = [(-0.428)(1.97) + (0.9988)(E_{\text{x ray}})^{3.232}]/[1.97 + E_{\text{x ray}}{}^{3.232}] \ . \tag{42}$$

The SiLi quantum efficiency equation for x rays with energies >15 keV is defined by the following relation:

$$C_{QE} = 1.006 - 1.36 \exp(-874.13 E_{\text{x ray}}{}^{-1.98}) \ . \tag{43}$$

Equation (40) was used to calculate the number of x rays incident on and detected by a SiLi detector. This equation was modified to determine the number of x rays transmitted through an absorber. The calculation of transmitted x rays requires that the spectral and intensity distribution of x rays incident on the front surface of an absorber is known. This distribution can be calculated by modifying equation (40) by removing the SiLi quantum efficiency correction.

Removing the quantum efficiency from equation (40) yields:

$$dI_{0\lambda}/dt = f_{\phi}(E)\Omega N_e \ , \tag{44}$$

where $dI_{0\lambda}/dt$ is the number of x rays at wavelength λ per unit time, $f_\phi(E)$ is the emitted photon spectral and intensity distribution at the surface of the impact target, Ω is the solid angle of the x-ray detector, and N_e is the number of incident electrons per second interacting with the target. Integrating equation (44) leads to:

$$dI_{0\lambda} = f_\phi(E)\Omega N_e \, dt \quad . \tag{45}$$

This integration yields the result:

$$I_{0\lambda} = f_\phi(E)\Omega N_e \, t \quad . \tag{46}$$

Here, $I_{0\lambda}$ represents the x-ray spectral and intensity distribution in a solid angle Ω due to $N_e t$ electrons that are impacting a surface. Now, consider the case of attenuating the x-ray flux with an absorber of thickness (x) and density (ρ).

When a beam of x rays passes through an absorber, the beam is attenuated by the scattering and absorption of x rays by electrons in the absorbing material. In order to estimate the magnitude of attenuation, consider a beam of monoenergetic x rays of intensity (I_0) incident on a slab of absorber of density (ρ), scattering cross section (σ), the number of electrons per gram mass in the absorber is defined by n, and the infinitesimal thickness is dx. The decrease in the x-ray intensity due to penetration of the absorber can be expressed as[35] :

$$dI = -I\sigma\rho n dx \quad , \tag{47}$$

where I is the x-ray flux, σ is the x-ray scattering cross section, ρ is the density of the target material, n is the number of electrons per gram mass of target material, and dx is the infinitesimal thickness of target material. Combining like terms and integrating yields:

$$\int (dI/I) = -\int \sigma\rho n dx \quad , \tag{48}$$

$$\ln I = -\sigma\rho n x + C \quad . \tag{49}$$

The constant of integration (C) can be determined by evaluating the x-ray intensity at the front surface of the absorber; i.e., at $x = 0$. Now:

$$\ln I_0 = 0 + C = C \quad . \tag{50}$$

Substituting this result into equation (49) and simplifying results in:

$$\ln (I/I_0) = -\sigma\rho n x \quad . \tag{51}$$

Expressing equation (51) in its exponential form results in:

$$I/I_0 = e^{-\sigma\rho n x} \quad . \tag{52}$$

The term σn is defined as the mass absorption coefficient, μ_m. Making this substitution yields:

$$I/I_0 = e^{-\mu m \rho x} \quad . \tag{53}$$

The term $\mu_m \rho$ is defined as the linear attenuation coefficient, μ. Making this final substitution yields the familiar relationship:

$$I = I_0 e^{-\mu x} \quad . \tag{54}$$

Now the number of x rays transmitted through this absorber can be calculated by using:

$$I(E) = I_0(E)\, e^{-\mu(E)x} \quad . \tag{55}$$

$I(E)$ in equation (55) is the number of x rays of energy (E) transmitted through the absorber, $I_0(E)$ is the number of x rays of wavelength λ incident on the absorber, $\mu(E)$ is the linear attenuation coefficient, and x is the thickness of the absorber. Several tabulated data sources were identified that provide linear attenuation and mass absorption coefficients for elements and compounds over specific x-ray energy ranges.[26,27,38] As shown in figure 4, the linear attenuation coefficient ($\mu(E)$) is a strong function of x-ray energy.

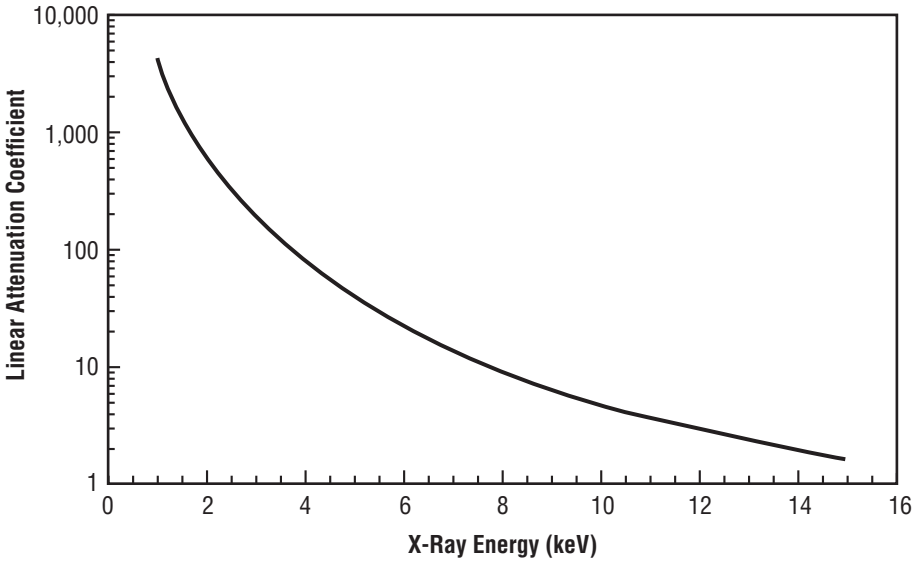

Figure 4. X-ray linear attenuation coefficient curve in carbon.

Now the transmitted x-ray spectral flux must be converted into an energy flux in order to determine absorbed dose,[28] resulting in:

$$I_E = I(E) E_E C_E \quad , \tag{56}$$

where I_E is the x-ray energy flux, $I(E)$ is the x-ray intensity at a specific energy (E), E_E is the x-ray energy at a specific energy (E), and C_E is a conversion factor from x-ray intensity to x-ray energy flux in MeV/cm^2*sec. Assuming that all of the x rays that are transmitted through the absorber will contribute to the absorbed dose, the absorbed dose can be determined as:

$$D = f_a I_E \ . \tag{57}$$

The term f_a is defined as:

$$f_a = C(\mu_a/\rho)_{\text{med}} \ . \tag{58}$$

The constant (C) is a conversion constant described as:

$$C = (1.6 \times 10^{-6} \text{ erg/1 MeV})(1 \text{ rad/100 ergs/g})(3.6 \times 10^3 \text{ sec/1 hr}) \ , \tag{59}$$

therefore,

$$C = 5.76 \times 10^{-5} \text{ rad*g*sec/MeV*hr} \ . \tag{60}$$

This value of the conversion constant (C) was determined by Henderson[25] and Fitzgerald.[28] The variable $(\mu_a/\rho)_{\text{med}}$ is the mass absorption coefficient for the medium in which the radiation energy is deposited. The variable μ_a is the linear absorption coefficient in cm^{-1}, and ρ is the density of the medium in which the radiation is deposited.[28]

The radiation studied in this investigation is low-energy x-ray radiation. The energy of these x rays is sufficient to affect only the skin or outer tissue regions of the body. Therefore, only the effects of radiation on the outer tissue will be discussed in this TM.

Radiation deposition in tissue is described by the term biological effect of radiation. The primary target of radiation in tissue is water, since 80 percent of all soft tissue is composed of water.[24] There are two categories of reactions that occur between radiation and water—primary and secondary. Primary reactions occur in a very short timeframe, on the order of 10^{-10} sec. Primary reactions introduce the formation of two new chemical species in water—free radicals. Free radicals are highly reactive due to the presence of an unpaired electron. One of the free radicals formed during radiation interaction with water is a hydrogen free radical. This is simply a hydrogen atom. The other free radical, a hydroxyl radical, is formed in significant numbers.

These free radicals are expressed as $\dot{\text{H}}$ for the hydrogen free radical and $\text{O}\dot{\text{H}}$ for the hydroxyl free radical. Combinations of these primary formed free radicals defines the secondary reactions. Secondary reactions occur during the following 10^{-5} sec after the passage of the incident radiation. Only three secondary reactions occur with high probability. These reactions are:

$$\dot{\text{H}} + \dot{\text{H}} \rightarrow \text{H}_2 \text{ (gas)} \ , \tag{61}$$

$$\dot{\text{H}} + \text{O}\dot{\text{H}} \rightarrow \text{H}_2\text{O} \text{ (water)} \ , \tag{62}$$

and

$$\dot{OH} + \dot{OH} \rightarrow H_2O_2 \text{ (hydrogen peroxide)} \quad . \tag{63}$$

The first reaction, equation (61), leads to the formation of molecular hydrogen gas. This reaction does not pose a significant threat to the tissue. The second reaction, equation (62), produces water, which is harmless to the tissue. The problem is the formation of hydrogen peroxide by the third reaction, equation (63). Hydrogen peroxide is a poison to cells. Gollnick[24] further states that a hydrogen atom could be dropped from the hydrogen peroxide to form peroxide that attacks other bioorganic molecules. This attack may prove fatal to the tissue cell. Blatz[39] states that safe dose levels for skin reactions are not known. Indications are that dose levels of 400 to 1,000 rads, absorbed in a duration of 1 to 3,600 sec (1 hr), could produce loss of hair and reddening of the skin due to blood vessel reactions. Hair and skin may return to normal after several weeks, with possible tanning of the skin. Doses of 1,000 to 1,500 rads could produce reddening and browning of the skin with subsequent scaling of the outer layers of skin. Hair may return with permanent tanning of the skin. The skin could be thinned and dry and subsequently easily injured. Doses of 1,500 to 5,000 rads in 3,600 sec could produce reddening and scaling of the skin and the possible appearance of raw, moist areas that last up to 2 weeks. Permanent skin damage is probable. Doses in excess of 5,000 rads in 3,600 sec could produce raw areas that may not heal. Surgical removal of the affected areas may be necessary.

Two specific types of x-ray detectors were used in this investigation—TLD's and a SiLi-drifted detector. The detector systems were selected for their ability to measure a specific x-ray environment. The TLD's were used to measure the absorbed dose in the high-intensity, low-energy x-ray environment generated by operation of the ISWE. A SiLi detector does not function well in a high-intensity x-ray environment and could not be used simultaneously with a TLD. The SiLi detector was used to accumulate x-ray spectra in a low-intensity x-ray environment generated by a low electron beam current electron source. The TLD's can be used in the low-intensity x-ray environment but exposure times on the order of years would be required to produce measurable results. The energies of the x rays produced by the ISWE electron source and the low electron beam current source were identical. Selection of the proper x-ray detector was critical to this investigation.

When a dielectric solid is exposed to ionizing radiation, or ultraviolet (UV) light, a varying percentage of the liberated electrons may become trapped at certain imperfections in the lattice. These imperfections are called electron traps. If the temperature is low and the traps are deep enough, they may remain trapped for hundreds or thousands of years before they are released by a sufficient stimulation, which increases their probability of escaping from the traps. Stimulation usually consists of the transfer of optical or thermal energy to the dielectric.[40] The return of the electrons to the stable state, which is called annealing, is associated with a release of energy. This energy, most of which is thermal, results in a minute temperature increase during annealing. A small fraction of the energy, however, may be released as visible or UV light, which can be observed as a transient glow of the preirradiated crystal or glass at a characteristic temperature during heating. This effect is called thermoluminescence.

The interaction of ionizing radiation with the phosphor results in the transfer of sufficient energy to electrons in the valence band, transferring them to the conduction band. A varying percentage of the liberated electrons recombine within a very short time with activators, releasing some of its energy in the form of light. This process is referred to as fluorescence.

The remaining electrons are captured in the electron traps. If the traps are not very deep, detrapping and recombination may already occur at a substantial rate around room temperature, resulting in a short half-life of the stored energy. This effect is usually called phosphorescence. Only if the traps are deep enough to result in sufficient storage stability at room temperature is the effect called thermoluminescence. In the case of thermoluminescence, transfer of thermal energy can liberate the trapped electrons.[40]

Liberation of trapped electrons results in several possible interactions, each of which produces photon emission. The photon emission intensity (Φ) of the TLD phosphor during heating can be described as[40]:

$$\Phi = -c\ dh/dt\ . \tag{64}$$

In equation (64), c is a proportionality factor, h is the number of electrons in the conduction band, and t is time. The TLD phosphor is heated at a constant rate and the emitted photons are collected as a function of temperature in a glow curve. Figure 5 shows a glow curve of some common phosphors. The area under each glow peak is proportional to the number of trapped electrons and, therefore, to the dose of a given type of radiation. The data were normalized for maximum peak height. The intensity of the peak intensity is a function of several variables: phosphor pretreatment, activator concentration, heating rate, and linear energy transfer of the impinging radiation, among others.[39]

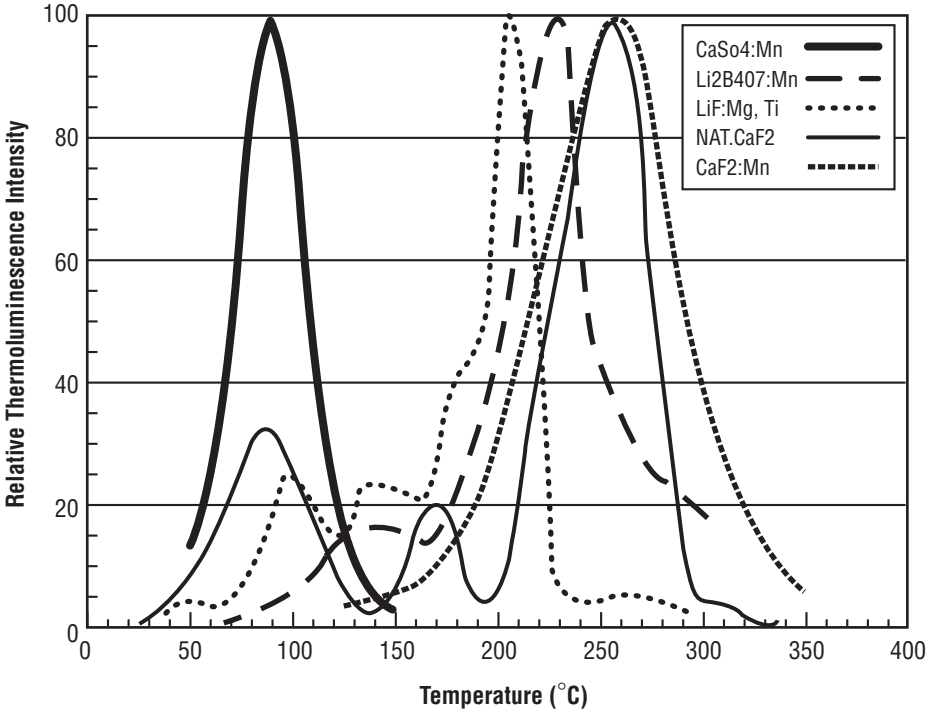

Figure 5. Thermoluminescence glow curves for some commonly used phosphors.

The SiLi-drifted detector consists of an *n*-*i*-*p* semiconductor arrangement. SiLi detectors are manufactured by depositing Li onto one side of *p*-type Si. The Li is thermally diffused into the *p*-type Si and further diffused by placing a potential across the system, thus driving the Li deeper into the *p*-type Si layer. The result of this diffusion process is the formation of three distinct layers. The *n*-type layer is Si with Li as a dopant, making the region rich in conduction band electrons.

The *i*-type layer is the region where the Li concentration is such that the region is intrinsic. The *p*-type layer is pure Si. The SiLi detector is operated with a bias across the intrinsic region, referred to as the depleted zone. This bias serves to sweep out the electron hole pairs formed by incident x rays before they can recombine.[41]

Consider an x ray of wavelength (λ) impinging the SiLi detector. The x ray interacts with atoms in the depleted zone and creates numerous electron hole pairs. The biased depleted zone sweeps the electrons toward the anode (*n*-type layer) and holes toward the cathode (*p*-type layer). This collection of current is processed by the detector as a voltage pulse. The height, or amplitude, of the voltage pulse is directly proportional to the energy of the incident x ray. This relationship can be described by the following:

$$E = cV \quad , \tag{65}$$

where E is the energy of the incident x ray, V is the amplitude of the voltage pulse, and c is the proportionality constant. This proportionality constant is determined by calibrating the SiLi detector and associated electronics prior to each use.

3. EXPERIMENTAL PROCEDURES

The first objective of the experimental portion of this investigation was to measure the radiation dose to the astronaut during the operation of the ISWE electron beam welding tool. This radiation dose measurement was accomplished using TLD's. Prior to this investigation, TLD's had not been used as dosimeters for low-energy x rays; i.e., ≤8 keV. Since this was the first time TLD's were used in this low-energy regime, calibration data were needed that relates TLD response to low-energy x-ray energy. This calibration, performed by the National Institute of Standards and Technology (NIST), produced a relationship between the TLD sensor response to low-energy x-ray irradiation and specific doses of low-energy x rays. After the NIST calibration of TLD sensors was complete, 15 TLD sensors were obtained from the U.S. Army Ionizing Radiation Dosimetry Center. These TLD's were used to measure the x-ray radiation dose due to operation of the ISWE electron beam welding tool.

Ten TLD sensors were placed in a vacuum chamber with the ISWE electron source. Eight of the ten TLD's were shielded by material identical to that worn by astronauts during EVA: Two were shielded by 2.8 mm of Lexan, two were shielded by 5.6 mm of Lexan, two were shielded by 8.4 mm of Lexan, and two were shielded by a sample of an astronaut's EVA space suit. Two were not shielded by material. Three of the five remaining TLD's were positioned at various locations on the exterior of the vacuum chamber to measure the potential radiation dose to the ground-based personnel operating or in the vicinity of the ISWE electron beam welding tool. Two TLD's were held as controls.

The TLD array was positioned in the ISWE vacuum test chamber at a distance of 584 mm (23 in.) from the location where electron beam impacts the metallic target and ≈160° with respect to the incident electron beam direction. This location, where the ISWE electron beam impacts the metallic target, is referred to as the weld pool. The metallic target for this test was aluminum. The vacuum test chamber was evacuated to a vacuum of 1×10^{-5} torr. The ISWE electron source was operated with an accelerating potential of 8 keV and an electron beam current of 76 mA. The total time the ISWE electron beam impacted the aluminum target was 1,800 sec (30 min). The 1,800-sec irradiation was performed in a series of short exposures, each short exposure lasting 180 sec (3 min), with 300 sec (5 min) between exposures to allow the aluminum sample to cool. After the 1,800-sec irradiation, the vacuum test chamber was repressurized with air, and the TLD array was removed. The TLD's were kept in a light-tight container for 86,400 sec (24 hr) at the recommendation of William Harris of the U.S. Army Ionizing Radiation Dosimetry Center prior to analysis. The TLD's were analyzed by the U.S. Army Ionizing Radiation Dosimetry Center.

A second TLD exposure was performed several weeks after the first exposure. The purpose of this second test was twofold: to verify the results of the first TLD exposure and to determine if an additional shielding configuration would be sufficient to reduce the radiation exposure to acceptable levels. The procedure for this second test was identical to the previous test. For this second TLD exposure, four TLD's constituted the TLD array that was placed in the vacuum chamber. The TLD array was positioned a distance of 584 mm from the weld pool. Two of the TLD's were shielded with 8.4 mm of Lexan, and two TLD's were shielded with a sample of the EVA space suit with two outer layers of Teflon® cloth. The NASA ground-based scientists and the author proposed using the Teflon cloth. The

addition of a Teflon cloth layer on the exterior of the space suit would serve a dual purpose; it would serve as a preventative measure guarding against molten weld droplets interacting with the space suit and reduce the radiation exposure to an EVA astronaut.

The second objective of the experimental portion of this investigation was to experimentally reproduce the ISWE exposure test geometry using a source of electrons other than the actual ISWE electron source, since it was no longer available. A Kimball Physics electron flood gun was used as the source of electrons. The electron flood gun is capable of producing electron beams of energies ranging from 1 to 50 keV. The electron beam currents are orders of magnitude lower than the ISWE, but this will serve as an advantage. The x-ray measurement device used was a SiLi-drifted detector instead of TLD's. The SiLi detects x rays and outputs data through a preamplifier and pulse amplifier to a multichannel analyzer (MCA). The MCA displays the x-ray data as a spectrum of x-ray intensity as the ordinate and x-ray energy as the abscissa. The SiLi detector and associated electronics were calibrated using the 5.9 and 6.5 keV gamma peaks from an ^{55}Fe source and the 1.48 characteristic aluminum peak.

The detector resolution was determined by calculating the full width half maximum (FWHM) of the ^{55}Fe peak at 5.9 keV. The FWHM resolution was nominally 235 eV. The SiLi detector preamplifier has a maximum processing speed of ≈200,000 counts/sec.[37] This means the SiLi detector can process 200,000 x rays per second.[37] If the x-ray flux exceeds this value, then x-ray information begins to be lost. The amount of lost information is proportional to the percent dead time indicated by the MCA.

Estimations indicate that the x-ray flux produced by the ISWE electron beam welding tool, operating at 76 mA, is on the order of 5×10^6 x rays/mm^2/sec at a distance of 584 mm (23 in.) from the electron impact site.[7] Therefore, any attempt to use SiLi to detect x rays during an ISWE test would result in erroneous x-ray spectral data. The use of an electron source that produces low beam currents allows the use of the SiLi detector to accumulate the x-ray spectrum generated by the interaction of electrons with metal. A vacuum test chamber at Marshall Space Flight Center (MSFC) was assembled to perform x-ray exposure testing. This test chamber was designed to reproduce the electron irradiation geometry identical to the ISWE TLD exposure tests. A drawing of this test geometry is shown in figure 6. This configuration was specifically designed to validate the analytical method for predicting x-ray spectra. Figure 6 shows a collimator positioned between the x-ray source and the SiLi detector. The purpose of the collimator was to filter any stray x rays originating from nontarget impact sites. This collimator was used when the SiLi detector was unshielded and the tests were performed to generate an experimental x-ray spectrum to compare to an analytical spectrum. The electron flood gun emits electrons at a 20° divergence angle. An aperture was included in the incident electron beam path to reduce the electron beam coverage area on the target. Using the aperture, the electron beam spot size on target is ≈12.7 mm (0.5 in.) diameter. Reducing the electron beam coverage area produces a geometry that approaches the ISWE experimental geometry. The electron impact target was positioned 584 mm (23 in.) from the SiLi detector.

The third objective in the experimental portion of this investigation utilized the experimental test system to produce x-ray spectral data to verify an analytical method for predicting x-ray spectra. Three metals—aluminum, copper, and molybdenum—were selected and each target was placed in the vacuum test chamber for electron irradiation. X-ray spectra were experimentally obtained using three specific incident electron energies: 8, 15, and 25 keV. The three targets were individually irradiated at each

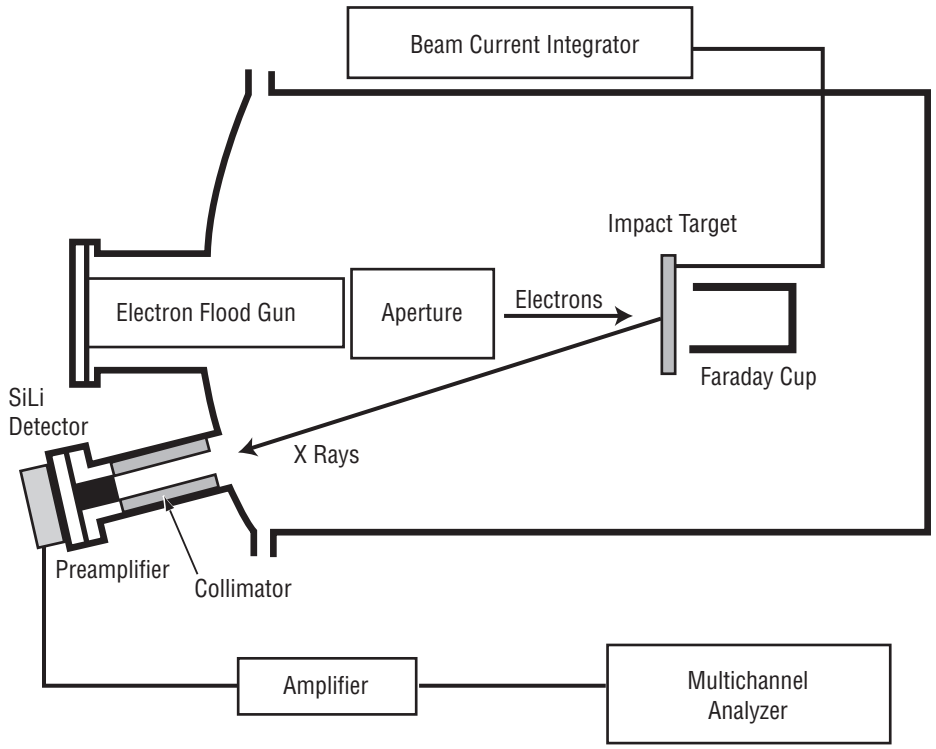

Figure 6. Vacuum test chamber at MSFC assembled to perform x-ray tests.

specific incident electron energy. The impact target sample holder was fabricated to allow the target material to be irradiated and BCI collected from the target. Periodically during the irradiation, the impact target was rotated out of the incident electron beam path. Once the target is out of the incident electron beam path, a Faraday cup measures the electron beam current. The results of this BCI comparison between the target and the Faraday cup define the correction factor (C_f) in equation (41). Equation (41) was used to normalize the experimental spectra to the analytical spectra. Results of this comparison are shown in section 5.

The fourth objective in the experimental portion of this investigation involved placing absorbers in front of the SiLi detector. The absorbers were identical to those used in the ISWE exposure test, described earlier in this section. The absorbers used in this experimental investigation were 2.8 mm of Lexan, 5.6 mm of Lexan, a sample of the EVA space suit, and a sample of the EVA space suit with two layers of Teflon cloth. The x-ray absorbers were positioned as close as possible to the SiLi detector. The electron flood gun was operated to produce an electron beam of energy 8 keV. The electron impact target was aluminum. The electron beam current was nominally 4 nA as measured from the impact target using BCI techniques. This electron beam current repeatedly provided a dead time value of <1 percent on the MCA. Figure 7 shows the position of the x-ray absorbers used in this investigation. The goal of this test was to replicate the previous ISWE exposure tests, and subsequently, verify the ISWE exposure TLD results. The ISWE exposure test, which was performed to meet objective one, did not include the use of secondary electron deflection techniques. The data accumulated to meet objective four also did not include the use of secondary electron deflection techniques.

The x rays transmitted through the various absorbers were collected by the SiLi detector and accumulated by the MCA. Accumulation times ranged from 3.6×10^5 sec (100 hr) to over 1.08×10^6 sec (300 hr), depending on the attenuation efficiency of the absorber. Higher absorber attenuation efficiencies required longer accumulation times. Spectra of x rays transmitted through the various absorbers used in this investigation are shown in section 5.

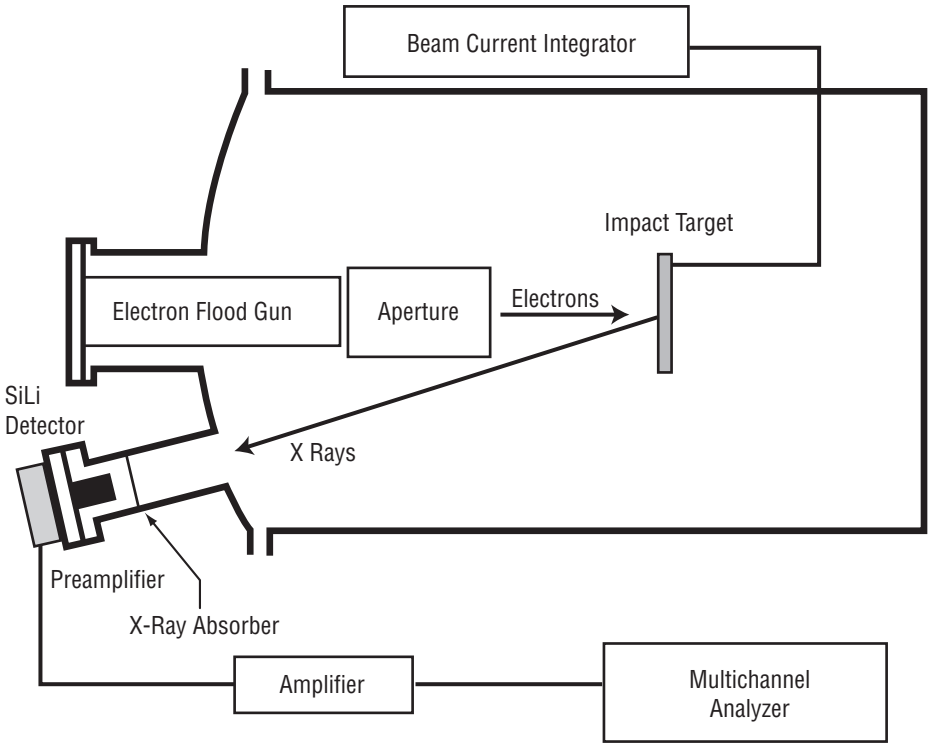

Figure 7. Vacuum test chamber at MSFC with x-ray absorber positioned between the x-ray source and the SiLi detector.

4. ANALYTICAL PROCEDURES

This analytical prediction method was designed to calculate the x-ray spectral and intensity distribution from monoenergetic electron-impact sources. X rays over the energy range from 1 to 8 keV were analytically propagated through various shielding materials, representative of an astronaut's EVA space suit. This resulted in the characterization of x rays transmitted through these various shielding materials. Having calculated the spectral and intensity distribution of these transmitted x rays, the assumption was made that all x rays transmitted through the shielding materials were absorbed by man. This assumption allowed for the calculation of the absorbed dose in man, due to the absorption of the transmitted x rays. This investigation concentrates on the x-ray spectrum generated by 8-keV electrons incident on aluminum. The first step in this analytical procedure was to calculate the x-ray spectral and intensity distribution generated when 8-keV electrons impact an aluminum target.

The x-ray spectrum at the surface of the electron-impact target was calculated using the software code ITS3. ITS3 consists of two codes: XGEN and TIGER. XGEN calculates the bremsstrahlung cross sections for the specific experimental parameters, and these cross sections are used in the TIGER code to calculate the x-ray spectrum at the surface of the electron-impact target. The output from ITS3 for the bremsstrahlung spectrum is the number of x rays in a predetermined energy bin. The size of the energy bin is determined, within limits, by the input file for ITS3. For this investigation, energy bins with a width of 0.4 keV were used. This was the narrowest energy bin that ITS3 could be programmed to output for an incident electron energy of 8 keV. ITS3 possesses a low-energy cutoff at 1 keV; therefore, all information from electrons and x rays with energy lower than 1 keV is not available. The input to ITS3 can be configured to output the number of x rays per energy bin in a given angular distribution. For this investigation, the angular distribution was assumed to be isotropic. Table 1 shows the raw output data of ITS3 for the case of 8-keV electrons incident on a thick aluminum target. The characteristic x-ray emission is also calculated by ITS3. The intensity of the characteristic x-ray emission is presented in units of x rays/sr per incident electron. Table 2 shows the raw output data of ITS3 for the characteristic x-ray emission for 8-keV electrons incident on an aluminum target. The number of x rays produced are normalized to one incident electron.

To generate an equation for the bremsstrahlung spectrum that relates x-ray energy to x-ray intensity, the data generated by ITS3, shown in table 1, are multiplied by geometry and experiment-specific constants to generate a data file unique for each experiment. For example, consider the case of 8-keV electrons incident on an aluminum target. The author empirically derived the following relationship to determine the number of x rays in each specific energy bin:

$$\text{Number of x rays} = [(I_{\text{ITS3}})(N_e t)^*(\Omega)^*0.001\ \text{MeV/keV}]^* \int_{E_l}^{E_h} dE \quad , \tag{66}$$

Table 1. Output of ITS3 listing the number of x rays generated from 8-keV electrons incident on an aluminum target.

Energy Range (MeV)	X Rays per Incident Electron (X Rays/MeV-sr)
0.0080–0.0076	0.0000316
0.0076–0.0072	0.0001210
0.0072–0.0068	0.0002390
0.0068–0.0064	0.0003890
0.0064–0.0060	0.0005860
0.0060–0.0056	0.0007270
0.0056–0.0052	0.0010300
0.0052–0.0048	0.0013900
0.0048–0.0044	0.0017800
0.0044–0.0040	0.0022300
0.0040–0.0036	0.0027500
0.0036–0.0032	0.0034200
0.0032–0.0028	0.0044900
0.0028–0.0024	0.0005600
0.0024–0.0020	0.0067800
0.0020–0.0016	0.0008500
0.0016–0.0012	0.0155000

Table 2. The ITS3 output for the characteristic x rays generated from 8-keV electrons incident on an aluminum target.

Energy (keV)	X Rays per Electron (X Rays/sr)
1.48	0.000199

where I_{ITS3} is the number of x rays per incident electron in a specific energy bin from the software code ITS3, $N_e t$ is the total number of incident electrons impacting the target, Ω is the detector solid angle. The integral $\int_{E_l}^{E_h} dE$ in equation (66) is evaluated over each specific energy bin with E_h and E_l defined as the upper and lower bound on the energy bin, respectively. The values of I_{ITS3} used in this example are listed in table 1. If the following data are used, $N_e t = 1.648 \times 10^{13}$ electrons, and $\Omega = 5.6 \times 10^{-6}$ sr, then the number of x rays per energy bin can be calculated. The results of these calculations are shown in table 3. The data in table 3 were used to generate an equation for the calculated bremsstrahlung spectrum, relating x-ray energy to x-ray intensity. The x-ray intensity was chosen to be at the midpoint energy of the energy bin. A best-fit equation was determined, using standard curve-fitting software, to relate the x-ray energy and x-ray intensity. Correlation factor comparison and inspection of the equation plotted with the data were used to determine the best-fit equation. The best-fit equation for the data in table 3 is defined as:

$$\text{Counts} = 1{,}690.98 - 1{,}734.62 \exp(-0.744\mathrm{E}^{-1.59}) \quad . \tag{67}$$

Figure 8 shows the plot of this best-fit equation for the data in table 3. This best-fit equation is denoted as $I_{0\lambda}$ in equation (46). The number of incident electrons was 1.648×10^{13} and the detector solid angle was 5.6×10^{-6} steradians.

Table 3. Data table showing the calculated number of x rays in each specific energy bin.

Energy Range (MeV)	Number of X Rays Incident on SiLi
0.0080–0.0076	1.26
0.0076–0.0072	4.85
0.0072–0.0068	9.58
0.0068–0.0064	15.60
0.0064–0.0060	23.50
0.0060–0.0056	29.15
0.0056–0.0052	41.30
0.0052–0.0048	55.74
0.0048–0.0044	71.38
0.0044–0.0040	89.43
0.0040–0.0036	110.28
0.0036–0.0032	137.15
0.0032–0.0028	180.07
0.0028–0.0024	224.57
0.0024–0.0020	271.89
0.0020–0.0016	340.86
0.0016–0.0012	621.57

The analytically predicted characteristic x-ray data are manipulated in much the same way as the bremsstrahlung spectral data. The number of incident electrons from equation (41) is multiplied by the detector solid angle and this product is multiplied by $I_{ITS3–C}$ as:

$$\text{Number of x rays} = (N_e t)(\Omega)(I_{ITS3–C}). \tag{68}$$

The term $I_{ITS3–C}$ in equation (68) is the output from the software code ITS3 in units of characteristic x rays per incident electron. Using the same values for $N_e t$ and Ω that were used to calculate the bremsstrahlung spectrum shown in figure 8 and $I_{ITS3–C}$ from table 2 results in the value indicated in table 4. The number of incident electrons was 1.648×10^{13} and the detector solid angle was 5.6×10^{-6} steradians.

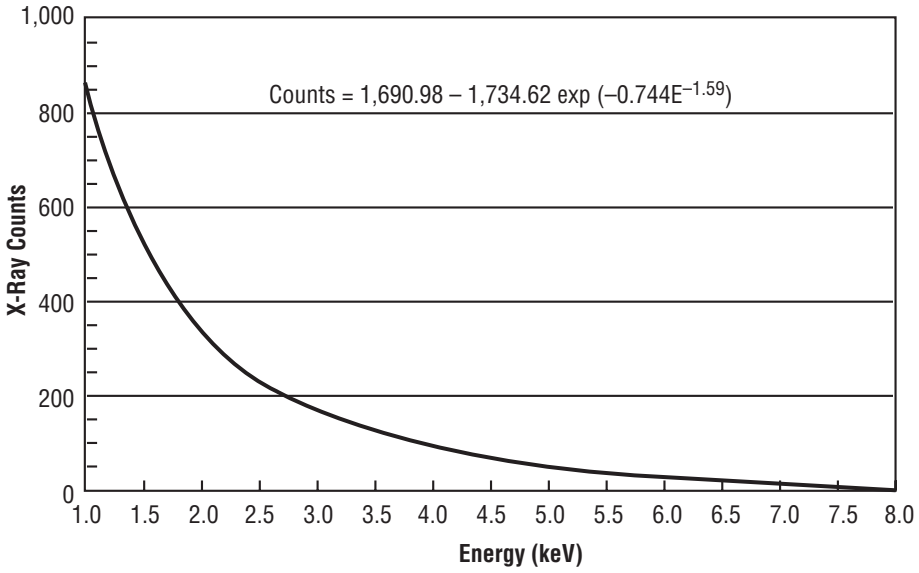

Figure 8. Calculated bremsstrahlung spectrum for 8-keV electrons incident on an aluminum target.

Table 4. Calculated characteristic x-ray intensity for 8-keV electrons incident on an aluminum target.

Energy (keV)	X Rays per Electron (X Rays/sr)
1.48	18,365

The total x-ray spectrum detected by the SiLi detector can be calculated by using equation (40) and substituting equation (67) for the term $f_{\phi}(E)N_e t\Omega$. The SiLi quantum efficiency is given by equation (42). Solving equation (40) yields the bremsstrahlung spectrum. The characteristic x-ray data are added to the bremsstrahlung spectrum data to produce the total x-ray spectrum.

Once the calculated x-ray spectrum was obtained, it was used to determine the x-ray spectrum of those x rays that are transmitted through various materials. Several x-ray absorbers were experimentally tested during the course of this investigation. Some of the shielding materials were single-layered materials and other shielding materials were multilayered. The procedure for calculating the transmitted x-ray spectrum through a single layer was slightly different than the procedure used when calculating transmitted x rays through multilayered shielding materials. This difference resides in the fact that some of the multilayered shielding materials were composed of cloth. The cloth materials contain a specific percentage of holes, allowing the incident x rays to penetrate without interaction. The procedure for calculating the transmitted x rays through a single-layered shielding material will be presented by describing the case of 2.8 mm of Lexan used as an x-ray absorber. The procedure for calculating the transmitted x rays through a multilayered shielding material will be presented by describing the case of a space suit used as a x-ray absorber.

Calculation of the x-ray spectral and intensity distribution transmitted through an absorber begins with defining the incident x-ray spectrum. The total x-ray spectrum, $f_{T\phi}(E)$, can be described by using equation (46) and substituting equation (67) for the term $f_{\phi}(E)N_e t\Omega$, then adding the characteristic x-ray line intensity from table 4. Now, $f_{T\phi}(E)$ is defined as the x-ray spectral and intensity distribution at a distance of 584 mm from the electron impact site for an electron fluence, $N_e t$. This relationship is expressed as:

$$f_{T\phi}(E) = I_{0\lambda} + I_{C\lambda} \ , \tag{69}$$

where $I_{0\lambda}$ is the bremsstrahlung spectrum described by equation (46), and $I_{C\lambda}$ is the characteristic line intensity described by equation (68).

This spectrum is normalized to an equivalent ISWE exposure by first reducing the spectrum to units of counts per incident electron as:

$$f'_{T\phi}(E) = f_{T\phi}(E)/N_e t \ . \tag{70}$$

Next, the spectrum, $f'_{T\phi}(E)$ is multiplied by the total number of electrons that impacted the aluminum target during a typical ISWE TLD exposure test. The number of electrons that interacted with the weld target was determined using the electron beam current of 76 mA and the ISWE operation time of 1,800 sec. Using the constant of 1.6×10^{-19} C/electron and recognizing that 76×10^{-3} A is equivalent to 76×10^{-3} C/sec results in:

$$76 \times 10^{-3} \text{ C/sec} \ / \ 1.6 \times 10^{-19} \text{ C/electron} \times 1{,}800 \text{ sec} = 8.55 \times 10^{20} \text{ electrons} \ . \tag{71}$$

The function $f'_{T\phi}(E)$ is multiplied by 8.55×10^{20} electrons to get:

$$f_{(\mathrm{ISWE})\phi}(E) = f'_{T\phi}(E) * 8.55 \times 10^{20} \text{ electrons} \quad . \tag{72}$$

The function $f_{(\mathrm{ISWE})\phi}$ is the x-ray spectral and intensity distribution during an 1,800-sec (30-min) ISWE operation that is deposited into a solid angle of 5.6×10^{-6} sr. The next step was to propagate this distribution through a shielding material.

Consider the case of 2.8 mm of Lexan as the shielding material. X rays transmitted through a material can be calculated using equation (55). Rewriting equation (55) for this case results in:

$$I(E) = f_{(\mathrm{ISWE})\phi}(E) \exp(-\mu(E)x) \quad , \tag{73}$$

where $\mu(E)$ is the linear attenuation coefficient for the shielding material (Lexan), and x is the thickness of the shielding material in centimeters. The linear attenuation coefficient, $\mu(E)$, for Lexan was not tabulated in any of the available resources. Acquisition of the linear attenuation coefficient for Lexan was accomplished by using the mass attenuation coefficient (μ/ρ) for carbon. The carbon mass attenuation coefficient was multiplied by the density of Lexan, 1.2×10^{-3} mg/mm^2 (1.2 g/cm^3) to obtain an approximation for the Lexan linear attenuation coefficient. The general equation for calculating this modified linear attenuation coefficient is described by:

$$\mu(E)_x = [\mu(E)_1/\rho_1][\rho_x] \quad , \tag{74}$$

where $\mu(E)_x$ is the nontabulated linear attenuation coefficient of the desired material, $[\mu(E)_1/\rho_1]$ is the tabulated mass attenuation coefficient of the known material, and ρ_x is the density of the desired material.

The chemical formula of Lexan is $C_{16}H_{14}O_3$, indicating the major constituent is carbon. The density of Lexan was found to be 1.2×10^{-3} mg/mm^2 (1.2 g/cm^3).[42] Using this calculated linear attenuation coefficient for Lexan and the thickness of 2.8 mm, the number of x rays transmitted through this Lexan thickness can be calculated.

The procedure for calculating the transmitted x-ray spectrum through a multilayered shield is slightly different than the procedure described for a single-layered shield. Consider the sample of a space suit used as an x-ray radiation shield. The space suit used was composed of multiple layers of various materials. Figure 9 describes the composition of the space suit used in this investigation. Some of the layers are porous and should transmit some percentage of the incident x rays without interaction. The layers identified as having measurable porosity were Beta® cloth and Dacron®. The remaining layers were assumed to be solid layers, for the purposes of calculating the x-ray attenuation.

Determination of the percent porosity was accomplished using a collimated light source and a radiometer. The intensity of the collimated light source was measured at a specific distance using the radiometer. Multiple measurements were obtained to ensure the light intensity was constant. Each porous layer in the space suit was placed between the light source and the radiometer, as close to the radiometer as possible.

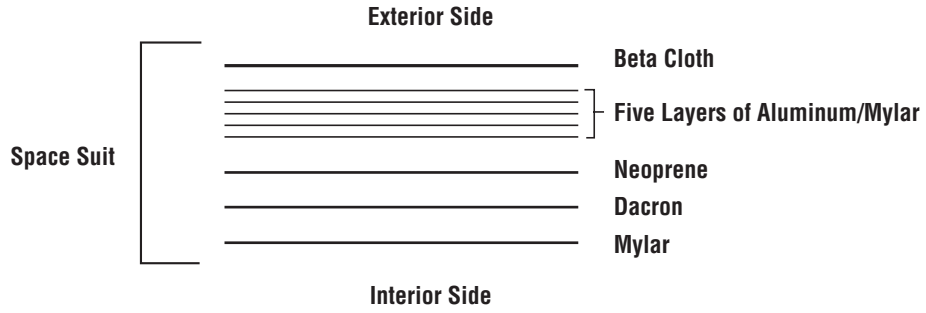

Material	Thickness (mm)
Beta Cloth	5.3×10^{-3}
Aluminum/Mylar	7.62×10^{-4} per Layer
Neoprene	2.03×10^{-3}
Dacron	2.54×10^{-3}
Mylar	2.54×10^{-3}

Figure 9. Composition of the space suit used in this investigation.

The assumption was made that the porous layers will have some measurable percentage of holes, and these holes will transmit the incident light without interaction. Also, the author assumed the fibers comprising these layers will be completely opaque to the incident light. Multiple measurements were obtained with the porous layer covering the radiometer. The percent of porosity was determined by the ratio:

$$\text{Percent porosity} = (\text{Intensity with shield/Intensity without shield}) \times 100 \quad . \tag{75}$$

Now the transmitted x ray can be calculated through this porous layer. As an example, consider the outer layer of the space suit, commonly termed Beta cloth. Beta cloth is a fabric consisting of woven threads of borosilicate fibers. The porosity test described above indicated that 6 percent of the Beta cloth consisted of holes, allowing light to transmit; therefore, 94 percent of the Beta cloth was opaque to the incident light. This same ratio of holes to material was applied to x-ray transmission. The author believes this ratio underestimates the x-ray transmission, due to the wavelength differences in visible light and x rays. Using this ratio, the following expression was used to determine the number of x rays that passed through the Beta cloth without interacting:

$$I_1(E) = (0.06) f_{(\mathrm{ISWE})\phi}(E) \quad . \tag{76}$$

Similarly, the number of x rays that were transmitted through the Beta cloth but did not penetrate through the holes can be expressed as:

$$I_2(E) = (0.94) f_{(\mathrm{ISWE})\phi}(E) \exp(-\mu_\beta(E)x) \quad . \tag{77}$$

The term $\mu_\beta(E)$ in equation (77) is the linear attenuation coefficient for borosilicate. Now the total number of x rays that are transmitted through the Beta cloth layer is given by:

$$I_\beta(E) = I_1(E) + I_2(E) \quad . \tag{78}$$

The x-ray flux incident on the first layer of aluminized Mylar is now defined by $I_\beta(E)$. This procedure of calculating the transmitted x rays through individual layers continues until all the layers, shown in figure 9, were analyzed. Table 5 shows the percent porosity for porous materials and the density of the solid material for the individual layers of the space suit. Linear attenuation coefficients for Beta cloth (borosilicate), aluminum, Mylar, and Teflon were found in the literature.[26] The linear attenuation coefficients for neoprene and Dacron were calculated using equation (74).

Table 5. Characteristics of percent porosity and density for the individual space suit layers.

Material	Porosity (%)	Density (g/cm^3)
Beta cloth	6.00	2.23
Aluminum	–	2.70
Mylar	–	1.38
Neoprene	–	1.23
Dacron	18.45	1.14
Teflon cloth	17.00	2.25

Analytical propagation of the x-ray flux through these layers results in a spectral and intensity distribution of transmitted x rays. This distribution of transmitted x rays was used to calculate the absorbed dose in man. Recall from section 5 that the absorbed radiation dose during an 1,800-sec operation of the ISWE was measured using TLD sensors. The TLD sensor was designed as an array of TLD elements, each element shielded by various thicknesses of tissue-equivalent material. The thickness of the tissue-equivalent material was designed to determine the dose at a specific depth in the human body. Figure 10 shows a diagram of the TLD sensor and the tissue-equivalent shielding for each element. The TLD element shielding configuration of interest to this investigation was the element shielded by $0.07 mg/mm^2$ of Mylar. In order to compare the calculated absorbed radiation dose due to the transmitted x rays to the absorbed dose measured by the TLD's, the attenuation through the $0.07\text{-}mg/mm^2$ Mylar layer must be considered. The transmitted x-ray spectral and intensity distribution was calculated by using equation (55) with $I_0(E)$ defined as the x-ray distribution incident on the $0.07\text{-}mg/mm^2$ Mylar layer. The x-ray distribution transmitted through this thin Mylar layer was denoted as $I(E)$. The x-ray distribution, $I(E)$, was assumed to be totally absorbed by the TLD element. Calculation of the absorbed dose was accomplished using equation (56) to convert the x-ray distribution, $I(E)$, into an energy flux, I_E. Finally, equation (57) was utilized with the calculated energy flux to calculate the absorbed dose.

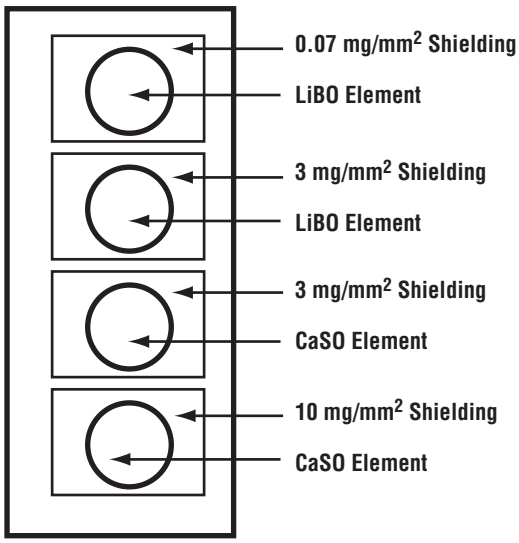

Figure 10. Diagram of TLD sensor used in this investigation.

5. RESULTS

The goal of this investigation was to determine adequate x-ray shielding for EVA astronauts operating the ISWE. Adequate x-ray shielding was defined in this investigation as a shielding configuration that reduces the astronauts' radiation exposure due to operation of the ISWE to ≈2 rem per 1,800-sec ISWE operation. The ISWE operation was defined as the ISWE operating for 1,800 sec with an electron beam energy of 8 keV, an electron beam current of 76 mA, and the weld target as aluminum. The goal of this investigation was successfully achieved.

The initial x-ray dosimetry using the ISWE tool was performed using TLD badges. One milestone of this investigation was that it produced the first known published dosimetry data using TLD's to measure absorbed dose from x rays with energies of 8 keV and lower.[31] Inaccessibility of the ISWE weld tool after completion of the TLD exposures required the development of alternative methods to verify the ISWE TLD results. The alternative methods included accumulating experimental x-ray spectra representative of the x-ray spectra generated by the operation of the ISWE and developing an analytical method to predict the x-ray spectra generated by the operation of the ISWE.

The analytical method developed in this investigation predicted that the x-ray spectral and intensity distribution from electron impact sources propagated this x-ray spectrum through various materials and calculated the absorbed dose from the transmitted x rays. The experimental method developed in this investigation was used to verify the analytical model and also verify the results of the ISWE TLD measurements.

NIST performed a series of x-ray exposures on TLD's to generate calibration data relating x-ray energy to tissue dose equivalence. NIST exposed the TLD's, provided by the U.S. Army Ionizing Radiation Dosimetry Center, to a known dose of x rays. For example, the L10 technique utilized x rays of mean energy 7.5 keV to expose the TLD's to doses of 43.82 and 262.93 milli gray (mGy).[31] This dose was referred to as Kerma, which is the absorbed dose in air due to the kinetic energy of all charged particles liberated by the incident radiation.[24] The results of this NIST exposure are detailed in table 6. Each NIST technique exposed the TLD's to a Kerma of 43.82 and 262.93 mGy. Tissue-equivalent plastic phantoms were used to obtain the value of tissue dose equivalents shown in table 6. After the NIST exposure, the TLD's were returned to the U.S. Army Ionizing Radiation Dosimetry Center for analysis.

A glow curve was generated for each TLD badge and integrated to determine a parameter denoted as mR*. The value of mR* is the area under a glow curve and is related to the tissue dose equivalent by the *k*-factor. The *k*-factor is the ratio of the tissue dose equivalent (mSv) divided by mR*. Figure 11 shows the *k*-factors calculated using the tissue dose equivalent value from the plastic phantom and the mR* value from the NIST exposed TLD. These *k*-factors were used to determine the tissue dose at a depth of 0.07 mg/mm^2 and are the calibration data points required to analyze the TLD measurements obtained in this investigation.

Table 6. Results of the NIST irradiation that were used to determine TLD badge response for photons.

NIST Technique	Mean Energy (keV)	Tissue Dose Equivalent (mSv) 0.07 mg/mm^2	3 mg/mm^2	10 mg/mm^2
L10	7.5	37.99	1.14	–
L10	7.5	227.96	6.83	–
L15	9.9	40.75	7.89	0.71
L15	9.9	244.75	47.33	4.21
L20	11.0	41.63	13.58	3.16
L20	11.0	249.78	81.51	18.93
L30	18.0	43.38	25.38	12.27
L30	18.0	260.30	152.50	73.62

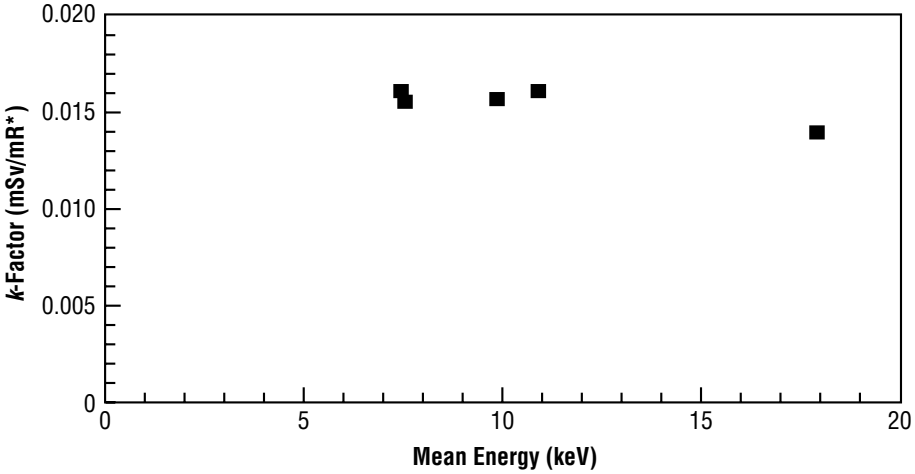

Figure 11. *k*-factor versus mean x-ray energy to assess the tissue dose at a depth of 0.07 mg/mm^2.

The initial dosimetry test used 15 TLD sensors obtained from the U.S. Army Ionizing Radiation Dosimetry Center. These TLD's were used to measure the x-ray radiation dose during operation of the ISWE electron beam welding tool. Ten TLD sensors were placed in a vacuum chamber with the ISWE electron source. Two TLD's were not shielded by absorbing material, two were shielded with 2.8 mm of Lexan, two were shielded with 5.6 mm of Lexan, two were shielded with 8.4 mm of Lexan, and two were shielded with samples of the extravehicular mobility unit (EMU) thermal micrometeoroid garment (TMG) restraint and bladder. The materials, identified as shields, were identical to those worn by astronauts during EVA. These 10 TLD's constitute the TLD array that were exposed, in vacuum, to x rays generated by the operation of the ISWE electron beam welding tool. Three of the five remaining TLD's were positioned at various locations on the exterior of the vacuum chamber to measure the potential radiation dose to the ground-based personnel operating the ISWE electron beam welding tool. The remaining two TLD's were held as controls. The TLD array was positioned at a distance of 584 mm from the location where the ISWE electron beam impacts the metallic target and ≈160° with respect to the incident electron beam direction.

Once the base vacuum of 1×10^{-5} Torr was achieved, the ISWE electron beam welding tool was operated for 1,800 sec. The electron impact target was aluminum. The electron energy was 8 keV and the electron beam current was 76 mA. The results of the TLD analyses are shown in table 7. The TLD's, in the array but not shielded by absorbing material, received excessive doses and could not be analyzed accurately by the U.S. Army Ionizing Radiation Dosimetry Center. The TLD's positioned on the exterior of the vacuum chamber did not receive a measurable dose. Therefore, the assumption was made that the stainless steel vacuum chamber sufficiently attenuated the x rays generated by the ISWE electron beam interaction with the aluminum weld target.

Table 7. TLD results from the first ISWE radiation exposure test.

Shielding Material	Dose (rem)
2.8-mm Lexan	22.06
2.8-mm Lexan	22.95
5.6-mm Lexan	2.25
5.6-mm Lexan	1.75
8.4-mm Lexan	0.18
8.4-mm Lexan	0.17
Space suit	9.70
Space suit	8.06

A second TLD exposure was performed using the ISWE electron beam welding tool. For this second TLD exposure, four TLD's were placed in the ISWE vacuum test chamber. Two TLD's were shielded with 8.4 mm of Lexan and two were shielded with a sample of space suit with two outer layers of Teflon cloth. The Teflon cloth was proposed by the NASA ground-based welding scientists and the author. This Teflon cloth served a dual purpose. The additional layer thickness would aid in the attenuation of x rays and would also provide a barrier to guard against molten weld droplets destructively interacting with the space suit. All other experimental parameters in this second ISWE exposure of TLD sensors were identical to the first exposure. Results of the TLD analyses for this second test are given in table 8.

Table 8. Results from the second ISWE radiation exposure test.

Shielding Material	Dose (rem)
8.4-mm Lexan	0.18
8.4-mm Lexan	0.17
Space suit with Teflon cloth	2.02
Space suit with Teflon cloth	2.64

This series of tests, using the ISWE hardware, indicated that the TLD measurements were repeatable. These tests also indicated that two layers of Teflon cloth placed on the exterior side of the space suit would reduce the absorbed dose to acceptable levels. Shortly after this second ISWE TLD exposure, the ISWE hardware was returned to the Ukraine and the ISWE program at NASA was terminated. Believing that NASA will one day utilize the technology of electron beam welding in space, the author wished to continue research into the ISWE radiation shielding issue. Experimental verification of the ISWE TLD results was needed and a method was needed to allow future investigators to evaluate alternative shielding configurations. The remainder of this section describes the experimental and analytical method developed to verify the ISWE TLD results. These methods can be used to evaluate other candidate shielding materials for astronauts during EVA.

The vacuum test chamber described in section 3 was used to accumulate x-ray spectra using three specific incident electron energies: 8, 15, and 25 keV. Three targets—aluminum, copper, and molybdenum—were individually irradiated at each electron energy. An unshielded SiLi detector was used to accumulate the x-ray spectrum, produced by the electron-target interaction. The charge deposited in the targets by the incident electron beam was accumulated using BCI techniques. Accumulation of the deposited charge allowed determination of the number of incident electrons that interacted with the target. To account for the emission of secondary electrons, as a result of incident electron impact, a Faraday cup was positioned directly behind the target. The target was periodically rotated out of the incident electron beam path to allow the Faraday cup to collect electron charge. Multiple measurements of the target and Faraday cup currents yield the consistent result that the target current is lower than the Faraday cup current. Table 9 shows the percent difference between the target and Faraday cup BCI. The average difference, shown in table 9, was used as the correction factor (C_f) in equation (41). Now the experimental spectra can be used as a verification standard to gauge the accuracy of the analytically generated x-ray spectral and intensity distribution.

Table 9. Percent difference in BCI from the target as compared to identical measurements from a Faraday cup.

Metal	Electron Energy (keV)	Average Difference (%)
Aluminum	8	19.70
Aluminum	15	18.54
Aluminum	25	16.60
Copper	8	45.54
Copper	15	45.49
Copper	25	44.19
Molybdenum	8	54.13
Molybdenum	15	59.78
Molybdenum	25	61.01

Sulkanen[19] developed a method for predicting x-ray spectral and intensity distributions from electron impact sources. Sulkanen's method was studied for potential use in this investigation. Comparison plots of Sulkanen's method with the results of the ITS3 software and experimental data revealed that

ITS3 provides better results when compared to experimental spectra. Figure 12 shows the comparison between Sulkanen's method, ITS3, and experimental data. As a result of this comparison, ITS3 was selected as the software code to use in predicting the x-ray generation from electron impact sources. The experimental plot is an experimentally accumulated spectrum; the ITS3 plot was generated by using the ITS3 model, and the Sulkanen plot was generated using Sulkanen's model.

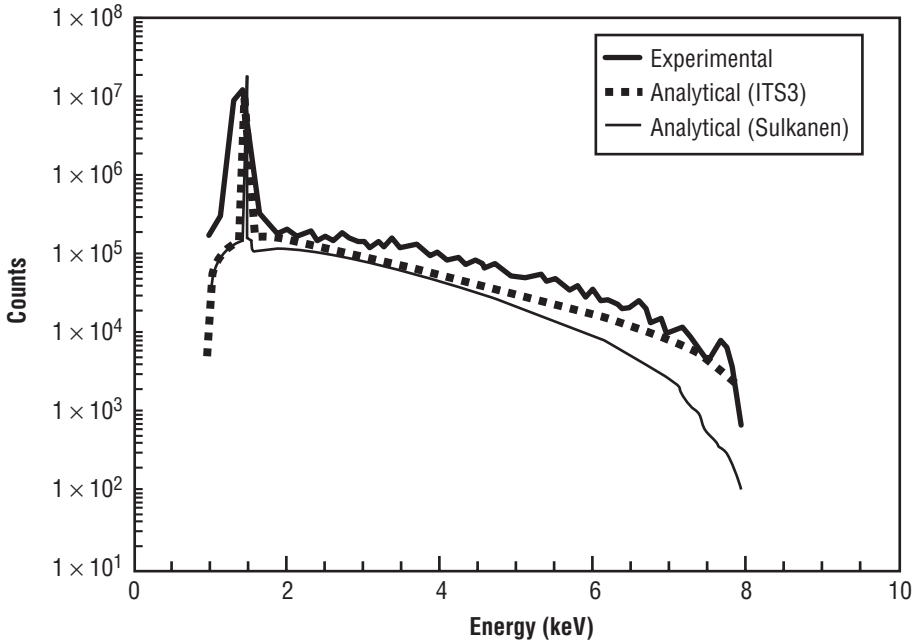

Figure 12. Comparison plot of x-ray spectra for 8-keV electrons incident on an aluminum target.

The analytical x-ray spectrum was calculated by starting with the integrated form of equation (40):

$$I_{0\lambda} = f_{\varphi}(E)\Omega N_e t C_{QE} \quad . \tag{79}$$

The function $f_{\varphi}(E)$ is the emitted bremsstrahlung spectral and intensity distribution at the surface of the impact target. The procedure for calculating $f_{\varphi}(E)$ is described in section 4. In order to compare the analytical x-ray spectrum to the experimental x-ray spectrum, the geometry-specific terms Ω, $N_e t$, and C_{QE} must be included.

The solid angle (Ω) for this investigation was 5.6×10^{-6} sr. The number of electrons incident on the impact target ($N_e t$) was calculated using equation (41). The SiLi detector used in this investigation has a specific quantum efficiency (C_{QE}) given by equation (42) for the x-ray energy range from 1 to 15 keV. Solving equation (79) for specific x-ray energies that are identical to the x-ray energies used in the experimental spectrum allows direct comparison of the analytical and experimental spectra. The analytical characteristic x-ray intensity was added to the analytical bremsstrahlung intensity, as described by equation (68) in section 4.

Experimental spectra were compared with the analytically predicted spectra to determine the accuracy of the analytical model. It was generally found that the continuum, or bremsstrahlung portion of the spectrum was in good agreement while the characteristic emission intensity of the analytical spectrum was consistently low when compared to experimental values. This result is common to published results.[19,23] A possible explanation of this consistent discrepancy in intensities resides in the statement by Pella et al.,[23] "Because parameters such as ionization cross section, target absorption factor, backscatter factor, and fluorescence yield are not known with sufficient accuracy, it is important to use measured x-ray output spectral distributions." The software package ITS3 does not calculate all possible x-ray transitions. Therefore, several experimental spectra contain small characteristic peaks that do not appear in the analytical spectrum. Figure 13 compares the experimental spectrum with the analytical spectrum for 8-keV electrons incident on an aluminum target. Calculated x-ray spectrum includes a correction factor to account for the SiLi quantum efficiency.

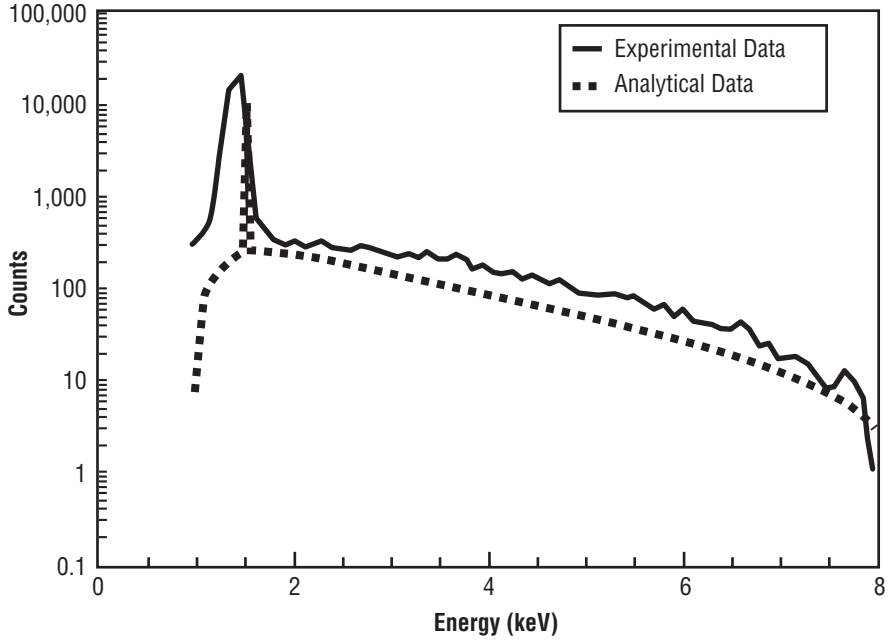

Figure 13. Comparison of experimental and analytical spectra of x rays generated by 8-keV electrons incident on an aluminum target.

The author defines the difference in the analytical and experimental x-ray spectra as the deviation factor. The deviation factor is calculated by the following:

$$\text{Deviation factor} = \text{Experimental data/Analytical data.} \tag{80}$$

The deviation factors calculated by equation (80) are shown in table 10. The deviation factors listed in table 10 are for the case of 8-keV electrons incident on an aluminum target. These deviation factors indicate that the analytical characteristic x-ray intensity is lower than the experimental characteristic x-ray intensity by a factor of 2. The ITS3 calculated the geometry of the experimental spectrum.

Table 10. Table showing the deviation factor between the experimental data and the ITS3 calculated data for x rays generated by 8-keV electrons incident on an aluminum target.

Energy (keV)	Deviation Factor	Energy (keV)	Deviation Factor	Energy (keV)	Deviation Factor
0.96	36.34	3.29	1.57	5.72	1.63
1.05	4.09	3.38	1.96	5.81	1.95
1.15	3.39	3.48	1.67	5.91	1.52
1.25	10.08	3.58	1.78	6.00	1.96
1.34	59.21	3.67	1.97	6.10	1.57
1.44	73.40	3.77	1.95	6.20	1.59
1.48	2.00	3.87	1.57	6.30	1.62
1.54	14.51	3.97	1.82	6.39	1.55
1.64	1.96	4.06	1.62	6.49	1.67
1.73	1.52	4.16	1.66	6.59	2.22
1.83	1.17	4.26	1.83	6.68	1.94
1.93	1.12	4.36	1.61	6.78	1.36
2.03	1.27	4.45	1.84	6.88	1.62
2.12	1.13	4.55	1.81	6.97	1.18
2.22	1.24	4.65	1.73	7.07	1.37
2.32	1.37	4.74	1.94	7.17	1.61
2.41	1.22	4.84	1.75	7.27	1.49
2.51	1.28	4.94	1.58	7.37	1.23
2.61	1.30	5.04	1.63	7.46	1.01
2.70	1.56	5.13	1.64	7.56	1.17
2.80	1.50	5.23	1.78	7.66	2.22
2.90	1.51	5.33	1.99	7.76	2.04
3.00	1.49	5.42	1.84	7.85	1.52
3.09	1.42	5.52	2.00	7.95	0.33
3.19	1.60	5.62	1.82	–	–

The analytical bremsstrahlung spectrum is also low by an average of 1.62 over the energy range of 1.64 to 8 keV. These results are in agreement with published results of Sulkanen[19] and Pella.[23]

With a few exceptions, the analytical x-ray intensity is constantly within a factor of 2 of the experimental x-ray intensity for x rays generated by 8-keV electrons interacting with aluminum. This same procedure for determining the deviation factor was used for comparing all unshielded SiLi detector experimental and analytical x-ray spectra. Figures 14 and 15 show the comparison of experimental and analytical x-ray spectra for 8-keV electrons incident on copper and molybdenum, respectively.

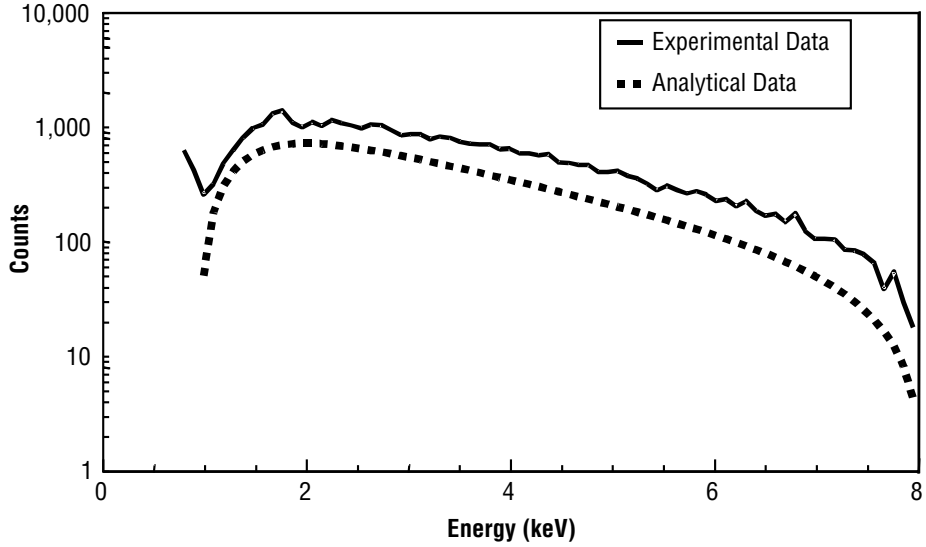

Figure 14. Comparison of experimental and analytical spectra of x rays generated by 8-keV electrons incident on a copper target.

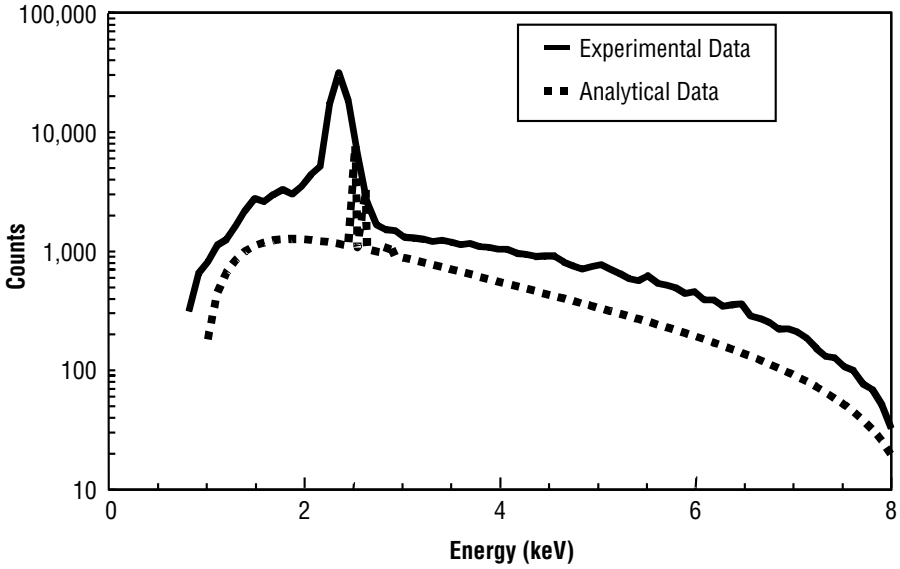

Figure 15. Comparison of experimental and analytical spectra of x rays generated by 8-keV electrons incident on a molybdenum target.

Comparison plots between the experimental and analytical x-ray spectra for 15- and 25-keV electrons incident on aluminum, copper, and molybdenum are also shown in figures 16 through 21. Deviation factors for aluminum, copper, and molybdenum irradiated with 8-, 15-, and 25-keV electrons were all on the order of 2, with notable exceptions for the characteristic intensities. A possible explanation for these consistently lower intensities in the characteristic peaks in the analytical spectrum was provided by Pella et al.[23] as insufficient accuracy in parameter definition.

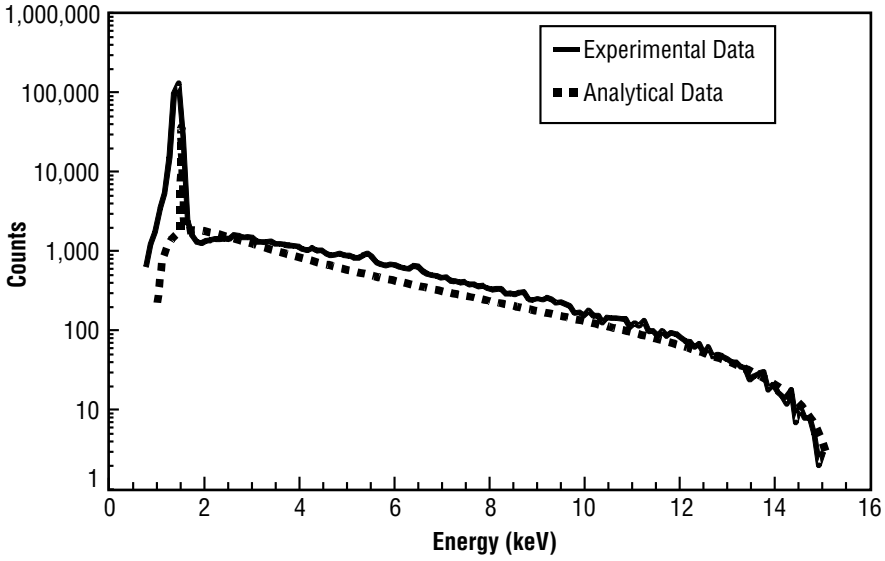

Figure 16. Comparison of experimental and analytical spectra of x rays generated by 15-keV electrons incident on an aluminum target.

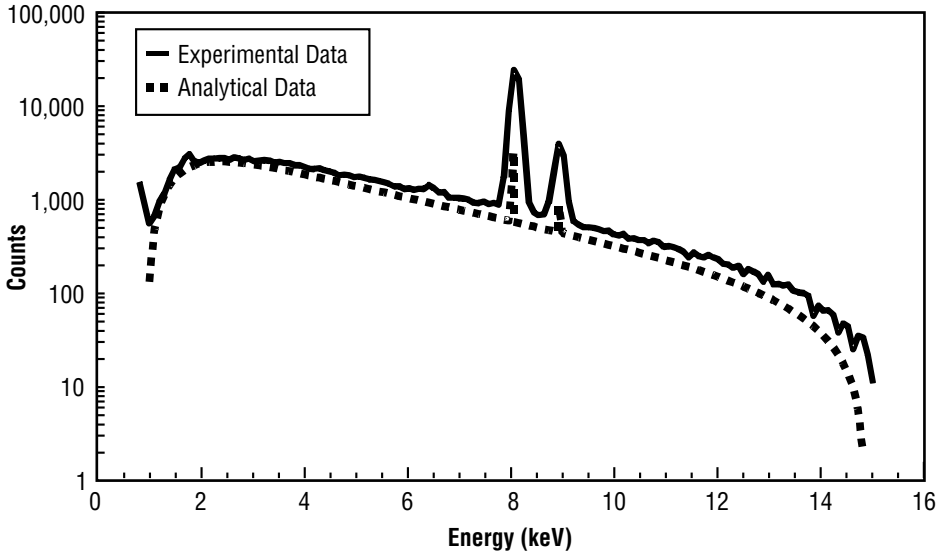

Figure 17. Comparison of experimental and analytical spectra of x rays generated by 15-keV electrons incident on a copper target.

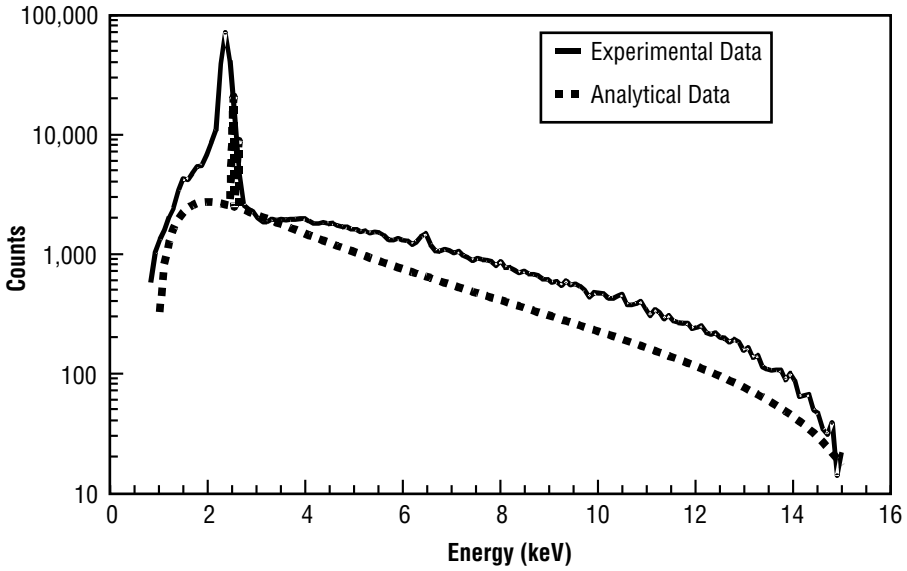

Figure 18. Comparison of experimental and analytical spectra of x rays generated by 15-keV electrons incident on a molybdenum target.

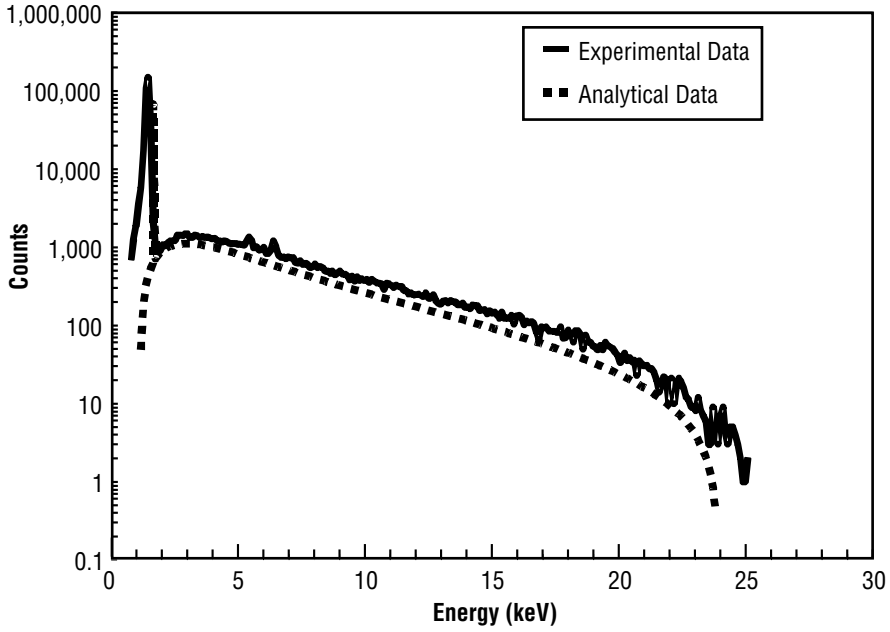

Figure 19. Comparison of experimental and analytical spectra of x rays generated by 25-keV electrons incident on an aluminum target.

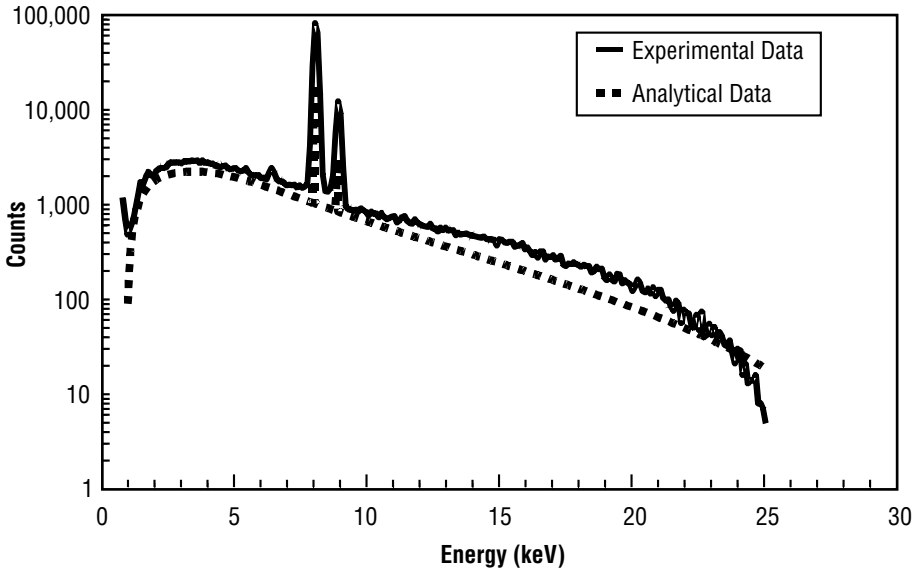

Figure 20. Comparison of experimental and analytical spectra of x rays generated by 25-keV electrons incident on a copper target.

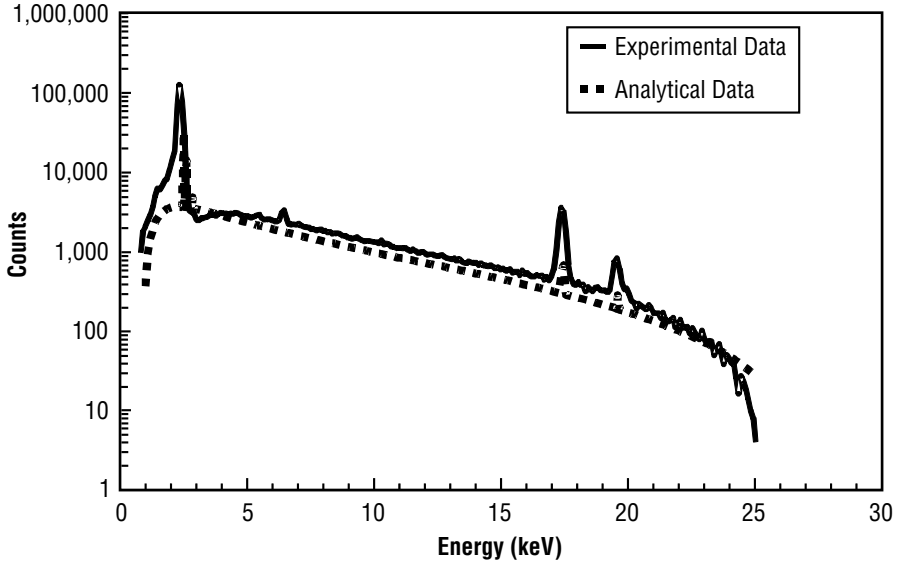

Figure 21. Comparison of experimental and analytical spectra of x rays generated by 25-keV electrons incident on a molybdenum target.

Once the analytical method was verified to be in agreement with experimental data for an unshielded SiLi detector, the investigation concentrated on x rays transmitted through various absorbers. The goal of this, and subsequent experimental tests utilizing x-ray absorbers, was to replicate the previous ISWE TLD exposure parameters in an effort to verify the ISWE TLD results. The differences in these experimental tests and the ISWE TLD exposures were (1) the ISWE electron beam current was stated to be 76 mA and the experimental tests used an electron beam on the order of 4 nA, and (2) the ISWE TLD test used TLD's to measure the x-ray-absorbed dose while the experimental test used a SiLi detector to accumulate an x-ray spectrum. The previous ISWE exposure of TLD's did not include the use of a collimator or magnets to deflect secondary electrons, therefore, neither did this set of experiments.

One of the primary questions to be answered was, "Would a measurable quantity of x rays be transmitted through the various absorbing materials?" This question was answered by positioning various absorbers between the x-ray source and the SiLi detector, as shown in figure 7. The first absorbing material used was 2.8 mm of Lexan. The Lexan was positioned as close as possible to the SiLi detector. Lexan is the material used for the astronauts' EVA helmet visor.

The electron beam energy for this set of experiments using a shielded SiLi detector was 8 keV. The impact target for this set of experiments was aluminum. The reason for this is to eventually normalize the results of these and subsequent tests to an equivalent ISWE exposure. The ISWE TLD exposure tests used an electron beam energy of 8 keV and a weld target of aluminum. Figure 22 shows the x-ray spectrum transmitted through 2.8 mm of Lexan after an irradiation of 3.8×10^{14}, 1.08×10^{15}, and 1.6×10^{15} 8-keV electrons.

The next x-ray absorber to be experimentally examined was also Lexan, but a thickness of 5.6 mm was used. The position of the 5.6-mm-thick Lexan was the same as indicated in section 3. As in the previous test, the electron flood gun was configured to produce an electron beam of 8 keV incident on an aluminum target. The electron beam current was measured to be 4 nA on the aluminum target. Figure 23 shows the transmitted x-ray spectrum using 5.6 mm of Lexan as an x-ray absorber. The number of 8-keV electrons incident on the aluminum target was 3.8×10^{14}, 1.08×10^{15}, and 1.6×10^{15}.

A sample of space suit was used as a x-ray absorber in the next set of experiments. A description of the individual space suit layers and a schematic of the layer configuration is shown in figure 9. The space suit was positioned in front of the SiLi, as indicated in figure 7. The electron flood gun was configured to produce an electron beam of energy 8 keV, and a beam current of 4 nA was measured on the aluminum target. Figure 24 shows the x-ray spectrum using the space suit as the x-ray absorber. The number of electrons incident on the aluminum target was 1×10^{16}, 1.85×10^{16}, and 2.93×10^{16}.

The final x-ray absorber to be experimentally tested in the MSFC vacuum test chamber was the space suit with two layers of Teflon cloth positioned on the exterior side of the space suit. The space suit and Teflon cloth layers were positioned as shown in figure 7. The electron flood gun was configured to produce an electron beam of energy 8 keV incident on an aluminum target. The electron beam current was measured to be 4 nA on the aluminum target. Figure 25 shows the transmitted x-ray spectrum using a space suit with two layers of Teflon cloth as an x-ray absorber. The number of electrons incident on the aluminum target was 8.97×10^{15}, 4.5×10^{16}, and 8.18×10^{16}.

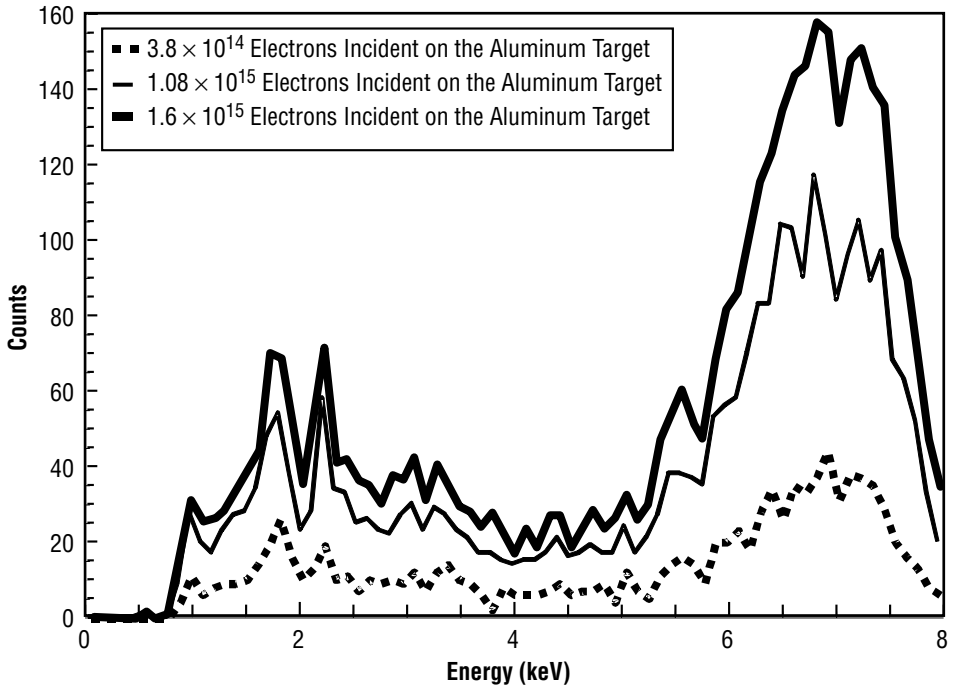

Figure 22. X-ray spectra transmitted through 2.8 mm of Lexan.

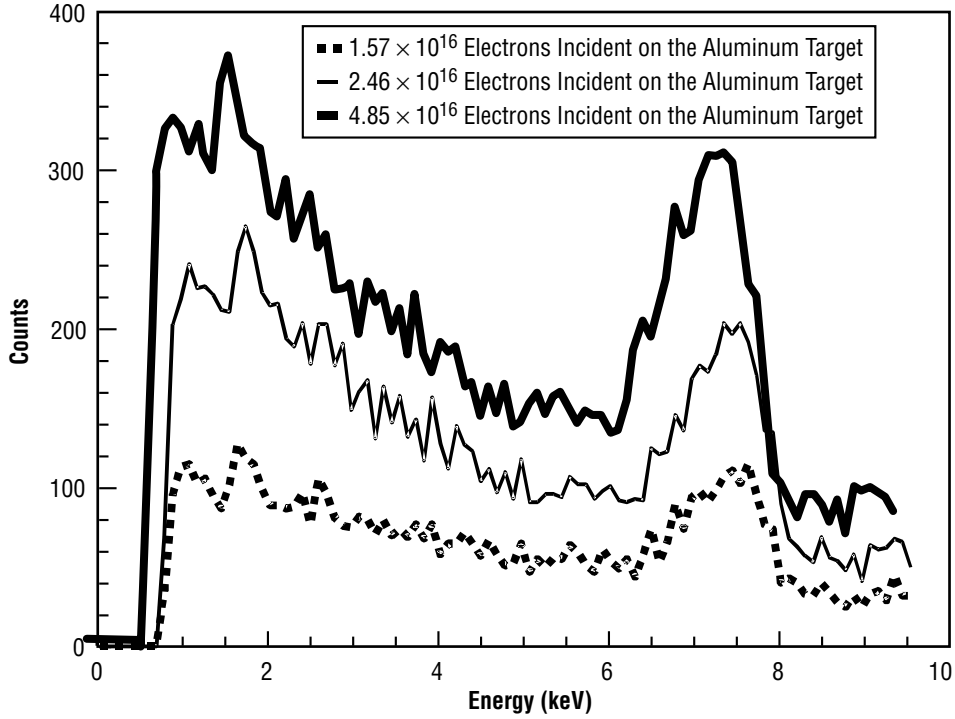

Figure 23. X-ray spectra transmitted through 5.6 mm of Lexan.

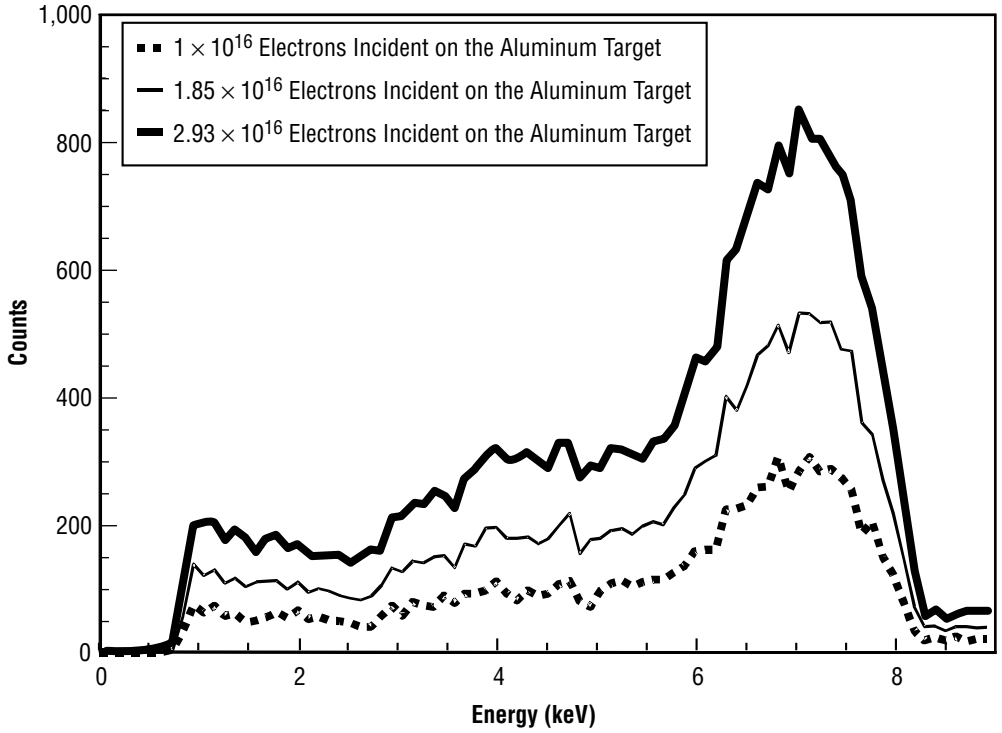

Figure 24. X-ray spectra transmitted through the space suit.

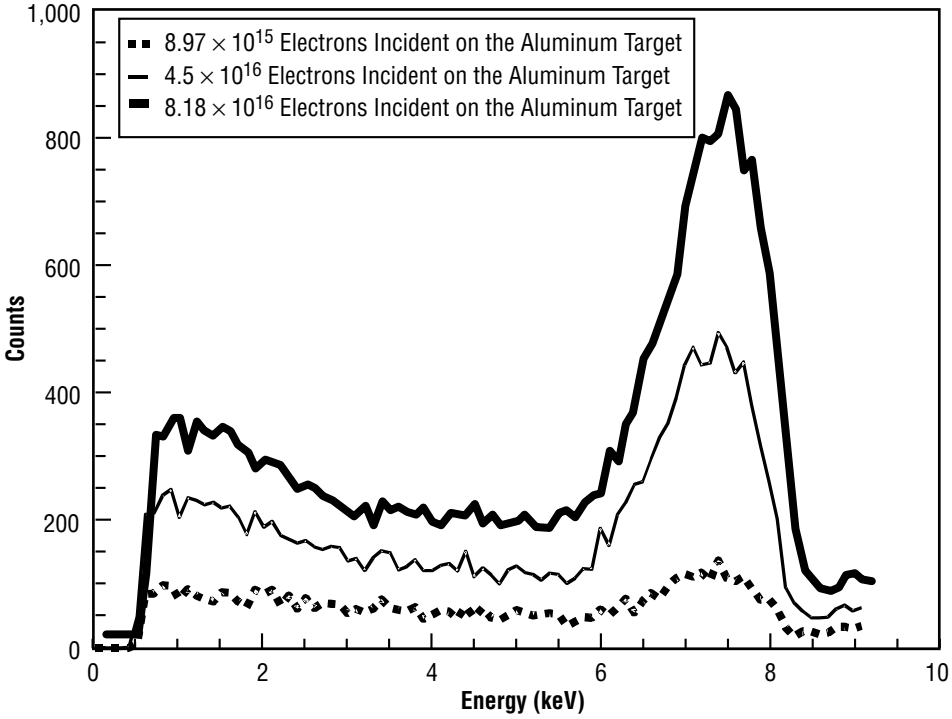

Figure 25. X-ray spectra transmitted through a space suit with two layers of Teflon cloth.

The spectra shown in figures 22 through 25 are raw experimental data. These spectra indicate that a measurable quantity of x rays will be transmitted through the various x-ray absorbers. The next step is to remove the background counts from these experimental spectra, normalize the spectra to units of counts per electron, and then compare the experimental spectra to analytical spectra.

Background counts were subtracted for each shielding configuration spectrum. Background subtraction techniques vary and can be subjective. Different background subtraction techniques were tried to determine the effect on the background-subtracted x-ray spectra. The largest percentage difference calculated in the background-subtracted spectra was 5 percent. This value is within the assumed error on the x-ray spectrum intensity. The error assumed on the intensity was the square root of the intensity for a given wavelength.

After the background counts were subtracted, the experimental x-ray spectra were normalized to units of counts per incident electron. Figure 26 shows the experimental x-ray spectra in units of counts per incident electron. Normalizing the x-ray spectra to units of counts per incident electron allows further calculations to be performed for any given electron fluence. These calculations include x-ray propagation through absorbers and conversion to absorbed dose.

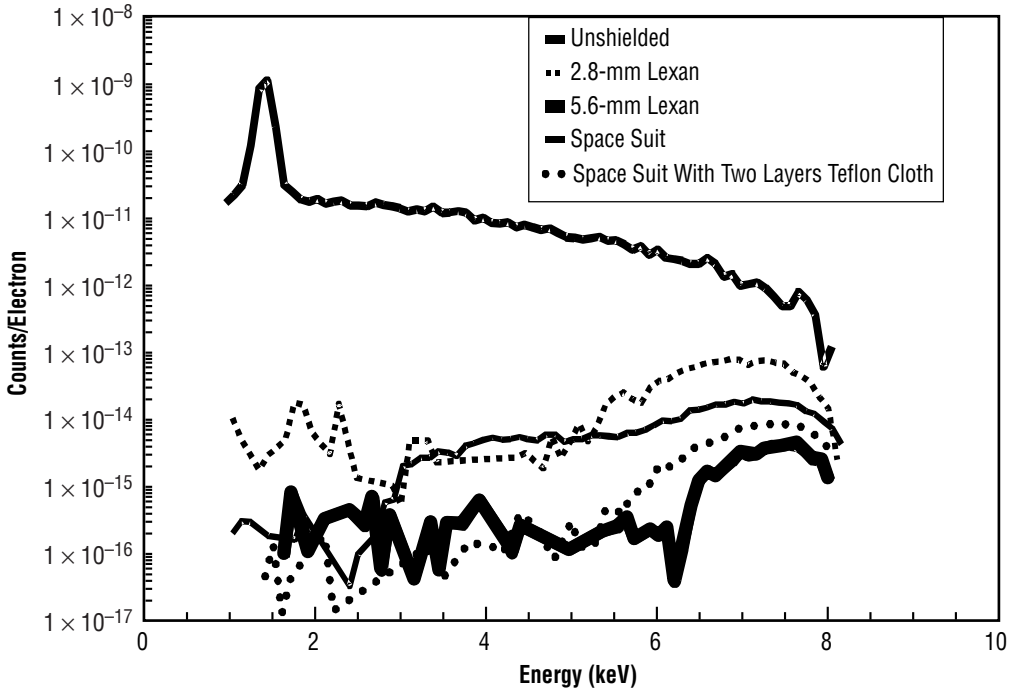

Figure 26. Comparison spectra of x-ray counts per incident electron for the different shielding configurations analyzed in this investigation.

Verification of the analytically predicted transmitted x-ray spectrum was achieved by comparing it to an experimentally accumulated transmitted x-ray spectrum. Deviation factors were calculated for the analytically predicted and experimentally accumulated transmitted x-ray spectra. The deviation factors were within a factor of 2 with the exception of the case where the two layers of Teflon cloth were added to the space suit. The general result was that the analytical method performed better modeling the x-ray spectrum transmitted through Lexan than through the space suit. Figure 27 shows the comparison of the experimental and analytical spectrum for x rays transmitted through 2.8 mm of Lexan. Both spectra were normalized to an electron fluence of 1.92×10^{15} incident on an aluminum target.

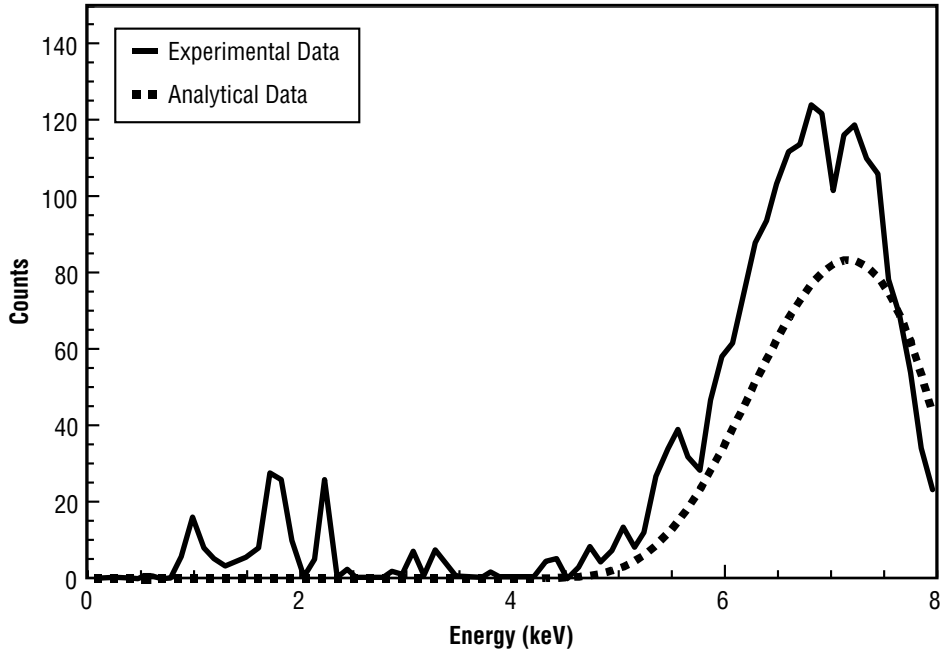

Figure 27. Comparison of experimental and analytical spectra of transmitted x rays through 2.8 mm of Lexan.

The author believes the reason the analytical method performed better when Lexan was attenuating the x rays was attributed to the single layer of Lexan as opposed to the multilayered space suit. Recall that Pella indicated the ionization cross section and fluorescence yield of photons are not well defined at low energies.[23] The combination of a multilayered x-ray absorber and inaccuracies in photon interaction parameters results in the analytical method deviating farther from the experimental data. Comparison spectra of the analytically predicted and experimentally accumulated transmitted x-ray spectra for the shielded cases of the 5.6-mm Lexan space suit and space suit with two layers of Teflon cloth are shown in figures 28–30.

One of the applications for experimentally accumulating and analytically calculating the x-ray spectral and intensity distribution is the determination of absorbed dose due to x rays transmitted through various shielding materials. This section describes the results obtained by converting the x-ray spectrum, whether experimentally accumulated or calculated, into absorbed dose in rem.

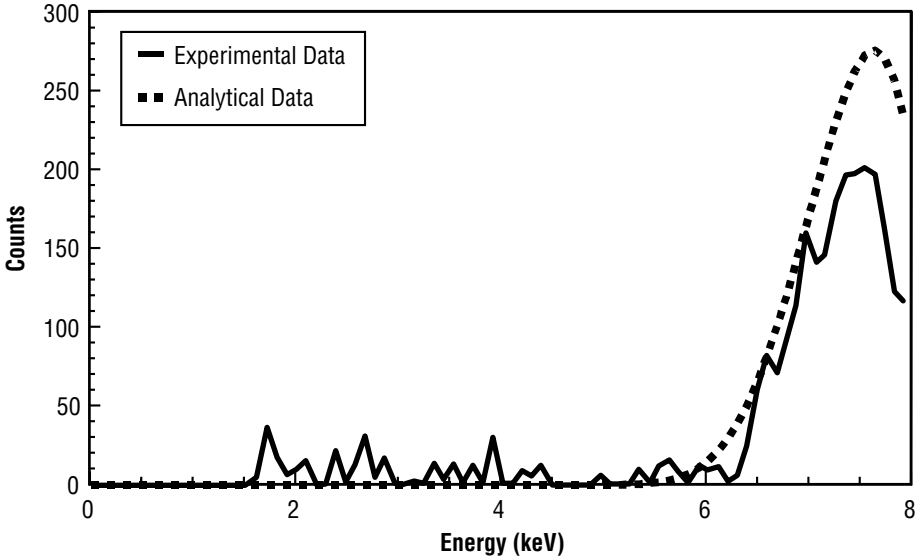

Figure 28. Comparison of experimental and analytical spectra of transmitted x rays through 5.6 mm of Lexan. Both spectra were normalized to an electron fluence of 4.85×10^{16} incident electrons.

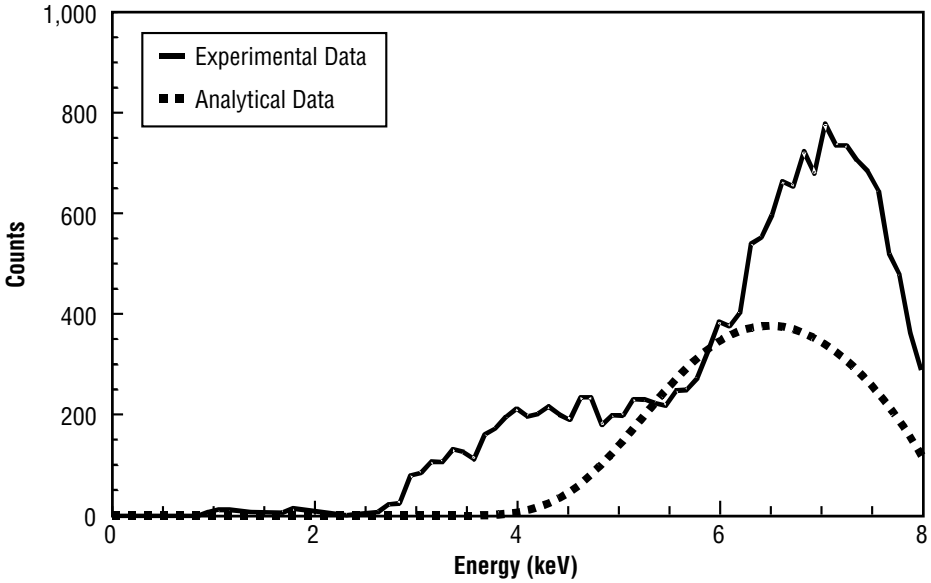

Figure 29. Comparison of experimental and analytical spectra of transmitted x rays through a sample of space suit. Both spectra were normalized to an electron fluence of 2.93×10^{16} incident electrons.

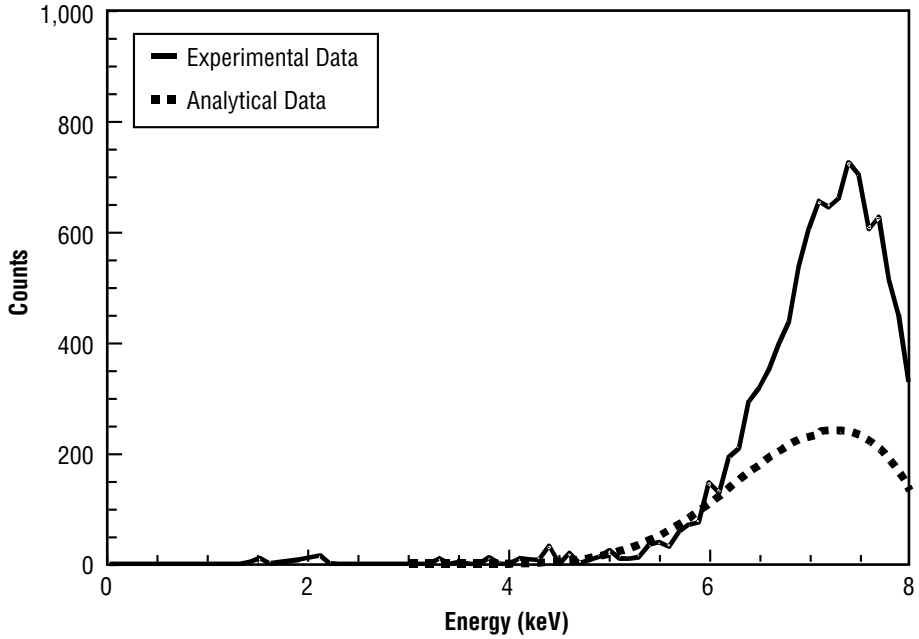

Figure 30. Comparison of experimental and analytical spectra of transmitted x rays through two layers of Teflon cloth over a sample of space suit. Each layer of Teflon cloth was 2.54×10^{-3} mm thick. Both spectra were normalized to an electron fluence of 8.18×10^{16} incident electrons.

Using the experimental data presented in figure 26 and normalizing to an ISWE-equivalent 1,800-sec exposure, the number of x rays as a function of energy that would be transmitted through a specific absorber during this 1,800-sec exposure can be determined. This normalization was accomplished by multiplying each spectrum by the number of electrons incident on the aluminum target during an 1,800-sec ISWE operation. The number of electrons was 8.55×10^{20} electrons.

The analytical x-ray spectrum was calculated using the procedure described in section 4. The analytical x-ray spectrum was normalized to an ISWE-equivalent exposure and propagated through a specific absorber. Now the experimental and analytical spectra can be compared.

Each TLD used in the ISWE TLD exposure possessed a thin Mylar film. This 0.07-mg/mm^2-thick Mylar film was representative of the tissue equivalence for skin. The objective of this section of the investigation was to use the experimental and analytical spectra to calculate the absorbed dose in a TLD element. Accomplishing this objective required that the attenuation through the 0.07 mg/mm^2 of Mylar be applied to the experimental and analytical x-ray spectra. Equation (55) was used to calculate the number of x rays transmitted through the 0.07 mg/mm^2 Mylar film. Now, the x-ray spectral and intensity distribution for x rays incident on a TLD element located a distance of 584 mm from the electron impact site. The electron beam characteristics are representative of an 1,800-sec ISWE operation with an 8-keV, 76-mA electron beam incident on an aluminum target.

The assumption was made that all x rays incident on the TLD element contribute to the absorbed dose, recorded by the TLD. With this assumption, the experimental and analytical spectra were converted from units of counts per unit energy to energy flux. Equation (56) was used to convert these spectra into

units of x-ray energy flux per unit energy. Figure 31 shows the comparison plot of the experimental and analytical x-ray energy flux incident on a TLD element and the parameters used to generate the data are described. The TLD was shielded by 2.8 mm of Lexan. The x rays were generated by an 8-keV electron beam with a beam current of 76 mA. The electron beam was incident on an aluminum target for 1,800 sec.

Using equation (57), the energy flux data in figure 31 is converted into units of dose rate per unit energy. The dose rate is in rem per hour. These data are shown in figure 32.

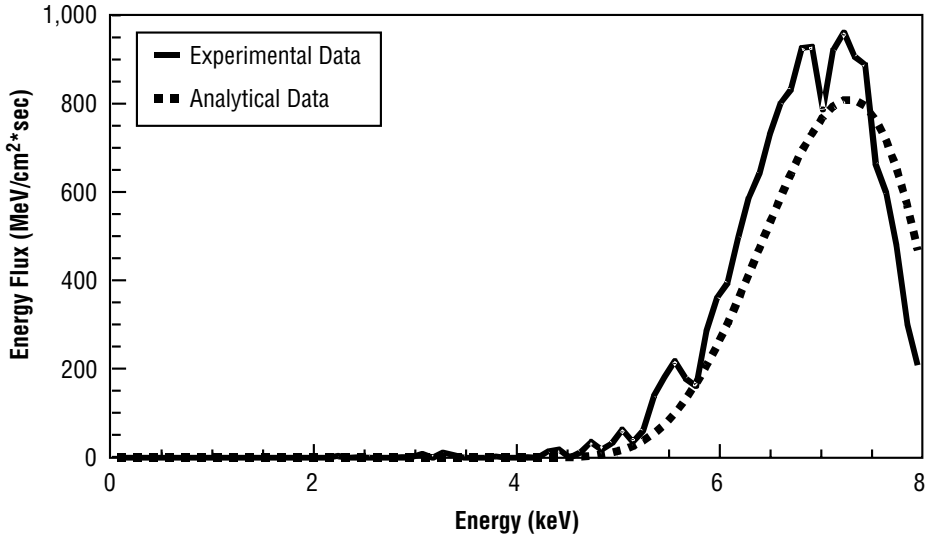

Figure 31. Comparison plot of the experimental and analytical x-ray energy flux incident on a TLD element shielded by 2.8 mm of Lexan.

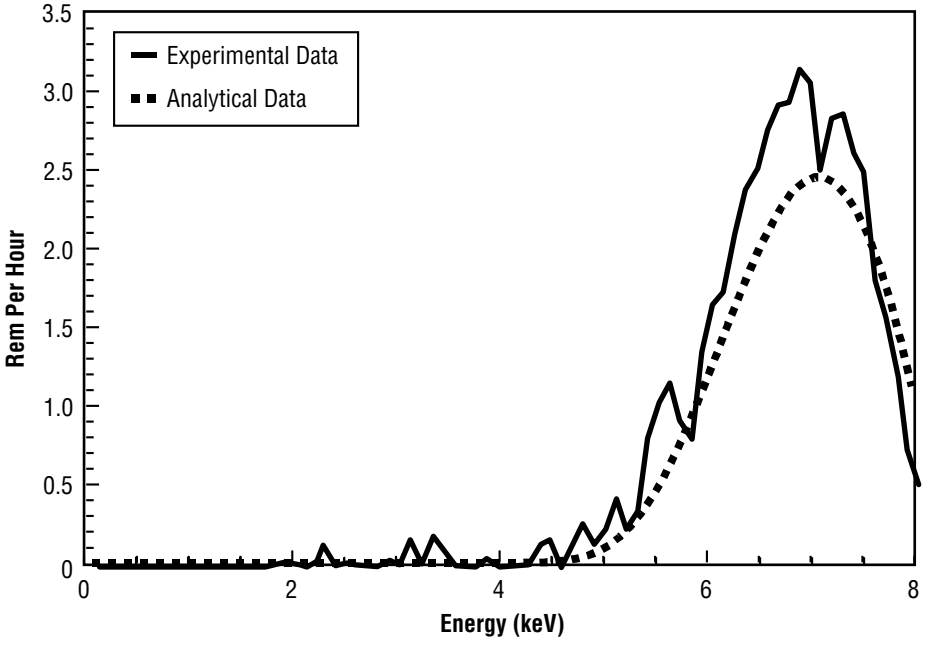

Figure 32. Comparison plot showing experimental and analytical dose rate as a function of energy for x rays incident on a TLD shielded by 2.8 mm of Lexan.

The total dose is calculated by summing the dose contributions as:

$$D_T = \sum_{I=E_l}^{I=E_h} D(E) \ , \tag{81}$$

where $D(E)$ is the dose rate at a specific x-ray energy, E_h is the upper limit of the x-ray energy, E_l is the x-ray energy lower limit, and D is the total absorbed dose rate in rem per hour. The results of this total dose calculation are shown in table 11. Analytical and experimental values were normalized to an 1,800-sec (30-min) operation of the ISWE electron beam welding tool with aluminum as a weld target. Electron beam energy was 8 keV and the electron beam current was 76 mA.

Table 11. Results of the dose calculations using the analytical method and experimental method compared to TLD measurements from the actual ISWE operation.

Absorber	Analytical (rem/30 min)	Experimental (rem/30 min)	TLD (rem/30 min)
0.28-cm Lexan	21.60 ± 1.30	26.63 ± 1.17	22.5 ± 4.50
0.56-cm Lexan	1.57 ± 0.07	1.21 ± 0.05	2.0 ± 0.40
Space suit	8.31 ± 0.34	12.34 ± 0.39	8.9 ± 1.80
Space suit with two layers of Teflon cloth	1.84 ± 0.08	2.33 ± 0.10	2.3 ± 0.46

This investigation focused on only one of the many applications of this x-ray prediction method; the determination of absorbed dose by analyzing an x-ray spectrum. This investigation details an analytical method to calculate the x-ray spectrum from electron interaction with metallic targets. This investigation further describes the techniques used to calculate absorbed dose from an x-ray spectrum. The general result is that the x-ray spectrum prediction model and experimentally accumulated x-ray spectrum can be utilized with a method for dose calculation to obtain a dose value that is in agreement with current state-of-the-art TLD dosimetry techniques.

The conclusion of this investigation resulted in a recommendation to the ISWE program office, located at MSFC, that the EVA astronauts operating the ISWE be outfitted with an extra external cover consisting of two layers of Teflon cloth. Two layers of Teflon cloth with a thickness of 2.54×10^{-3} mm (0.01 in.) and a denier of 400, construction warp of 100, and fill of 80 would be sufficient to reduce the absorbed radiation dose to ≈2 rem per 1,800-sec (30-min) operation. Denier is defined as the grams per 9,000 m of material. The construction warp is the largest value of threads per inch in a woven fabric. Fill is defined as the number of threads per inch in the direction orthogonal to the construction warp. These Teflon cloth layers would also provide protection to the EVA astronaut from molten weld droplets that could adhere to the space suit and catastrophically degrade the integrity of the space suit.

An additional recommendation was proposed to increase the Lexan thickness of the helmet visor assembly. The current Lexan thickness is ≈4.1 mm. A minimum thickness of 1.5 mm of Lexan should be added to the existing helmet visor assembly. This would reduce the absorbed radiation dose to the head and face to <2 rem per 1,800-sec operation. It was further recommended that this additional visor be attached to the helmet with VELCRO® to allow the additional Lexan shield to be easily removed. The logic associated with this recommendation was based on the possibility of metal vapor deposition from weld metals other than aluminum. If the additional Lexan shield became metal vapor coated, it could be removed and replaced with a clean Lexan shield.

Unfortunately, the ISWE program was terminated before this investigation reached completion. The proposed recommendations were not implemented, and NASA currently does not plan to utilize the ISWE technology in its space exploration initiative. The author believes that one day the ISWE technology will be required, and the results of this investigation will be available to better serve NASA's manned space program.

6. DISCUSSION

Near-term application of the ISWE electron beam welding tool is not in the NASA plan for the space exploration initiative. NASA has elected to pursue joining technologies that do not include the ability to join metallic interfaces by electron beam welding in space. The author believes that electron beam welding in space will need to be utilized if NASA is to successfully manufacture or assemble large structure hardware for extraterrestrial missions. Results of this investigation have proven that electron beam welding can be performed safely, from a radiation exposure viewpoint. The results of this investigation will remain in the NASA documentation library until such a time NASA decides to implement electron beam welding in space. This investigation produced several spinoff technologies, expanded the use of TLD's for radiation dosimetry, and reaffirmed proven fundamental physics relationships.

This investigation produced the first publication where TLD's were used to measure the radiation dose from low-energy x rays.[31] Prior to this investigation, TLD's were considered to lack sensitivity for the detection of x rays <10 keV. Undocumented popular opinion was that x rays <10 keV would be totally attenuated by the most modest of shielding materials.

Several papers were reviewed during this investigation that detailed radiation measurements of low-energy x rays and subsequent calculation of radiation dose from these measurements.[3,29] One of these papers was by Schollhammer.[29] Schollhammer was developing an in-vacuum electron beam welding tool in 1967.

The paper states recognition of a potential radiation hazard due to x rays generated by electron impact of metallic targets. Schollhammer provided conclusions that the radiation exposure was minimal. The author found the radiation measurement instrumentation used to detect and accumulate the x rays was questionable as to its sensitivity to detect low-energy x rays. Schollhammer did include a layer of stainless steel with the electron beam welding system of sufficient thickness to attenuate the x rays generated by the electron beam welding system. Calculations performed by Schollhammer indicated that the stainless steel shield provides sufficient x-ray attenuation to operate their in-vacuum electron beam welding tool.

A research agency of the Ukrainian government, PWI, manufactures an electron beam welding tool. This is the device that was leased by NASA and the instrument referred to as the ISWE electron beam welding tool in this investigation. PWI provided documentation indicating the radiation exposure during operation of the ISWE electron beam welding tool was very low.[3] Careful review of this document revealed some discrepancies. The document provided by PWI states the ISWE electron beam welding tool was operated with an electron acceleration potential of 8 keV and an electron beam current of 52 mA. A SiLi detector was reported to have been used to detect the generated x rays. This detector was positioned 700 mm from the electron impact site. The number of pulses accumulated by the SiLi detector was 200. A quick calculation indicates that the number of pulses is not accurate. Consider (1) an exposure time of 18.708 sec, (2) an electron beam energy of 8 keV, and (3) an electron beam current of 52 mA. The number of electrons emitted by the ISWE electron source and therefore the number of electrons incident on the stainless steel target can be calculated by:

$$(52 \times 10^{-3} \text{ C/sec})/1.6 \times 10^{-19} \text{ C/electron}) = 3.25 \times 10^{17} \text{ electrons/sec} \ , \tag{82}$$

and using an exposure time of 18.708 sec gives:

$$3.25 \times 10^{17} \text{ electrons/sec} \times 18.708 \text{ sec} = 5.85 \times 10^{18} \text{ electrons} \ . \tag{83}$$

Using equation (1) to calculate the x-ray production efficiency and assuming a Z of 26 for iron gives:

$$\xi = 1.3 \times 10^{-9} \ (26)(8{,}000) \ . \tag{84}$$

Solving for ξ in equation (84) gives:

$$\xi = 2.704 \times 10^{-4} \ . \tag{85}$$

Using an average value of bremsstrahlung radiation of 5.3 keV,[7] the energy per x ray can be calculated as:

$$(5{,}300 \text{ eV/x ray})(1.6 \times 10^{-19} \text{ J/eV}) = 8.48 \times 10^{-16} \text{ J/x ray} \ . \tag{86}$$

Assuming the ISWE electron beam welding tool operated at 8 keV and 52 mA, the power imparted to the stainless steel target was:

$$P_e = VA \ , \tag{87}$$

where P_e is the power imparted to the stainless steel target by the incident electrons, V is the accelerating voltage of the ISWE (volts), and A is the electron beam current (amps). Then:

$$P_e = 416 \text{ J/sec} \ . \tag{88}$$

The power of the emitted x rays can now be calculated as:

$$P_x = \xi P_e \tag{89}$$

or

$$P_x = 0.1125 \text{ J/sec} \ . \tag{90}$$

Now, the number of x rays emitted from the surface of the stainless steel target can be calculated. This number is given by:

$$N_x = (0.1125 \text{ J/sec})/(8.48 \times 10^{-16} \text{ J/x ray}) \ . \tag{91}$$

Solving for N_x gives:

$$N_x = 1.33 \times 10^{14} \text{ x rays/sec} \ . \tag{92}$$

The x-ray intensity at a distance of 700 mm from the target would be on the order of:

$$1.33 \times 10^4 \text{ x rays/sec})/2\pi r^2 = 4.32 \times 10^7 \text{ x rays/mm}^2\text{/sec} \quad . \tag{93}$$

Assuming an active area of the SiLi detector to be 12 mm^2 gives:

$$4.32 \times 10^7 \text{ x rays/mm}^2\text{/sec})(12 \text{ mm}^2) = 5.18 \times 10^8 \text{ x rays/sec} \quad . \tag{94}$$

Now, assuming an ISWE electron beam welding tool operation of 18.708 sec, the total number of x rays incident on the SiLi detector that would have interacted with the SiLi detector during the exposure time of 18.708 sec was:

$$(5.18 \times 10^8 \text{ x rays/sec})(18.708 \text{ sec}) = 9.69 \times 10^9 \text{ x rays} \quad . \tag{95}$$

The Ukrainian document states that 200 pulses were accumulated during the exposure time. The author assumed that 200 pulses is equivalent to 200 x rays counted. This quick calculation indicates that a discrepancy of ≈7 orders of magnitude in the number of x rays incident on the SiLi detector could potentially exist. The Ukrainian document uses the result of 200 pulses to calculate a radiation environment of 7×10^{-3} rads per hour during operation of the ISWE electron beam welding tool for the above-stated parameters. If a discrepancy exists in the number of x rays incident on the SiLi detector, then a discrepancy exists in the radiation dose absorbed during the operation of the ISWE electron beam welding tool.

During the months the Ukrainian scientists were working at MSFC, the author repeatedly inquired about details of this test report. The Ukrainian scientists strongly defended the accuracy of the document. Only after several radiation dosimetry tests were performed with results indicating a radiation environment of several rads per hour exists did the Ukrainian scientists begin to weaken in their defense of the document. In the author's last conversation with the Ukrainian scientists, a possible explanation for the large discrepancy was revealed.

The test report, "Protocol of Testing the Universal Technological Hardware," was released in December 1989. The experimental work was actually performed in 1984 while the Ukraine was still under the Soviet government. The Ukrainian scientists indicated that the x-ray detector used in the experiment was not a SiLi detector, as stated in the test report, but rather a German-made x-ray detector that dates to pre-World War II. The Ukrainian scientists also believed that this detector did not have the sensitivity to accurately measure the low-energy x rays generated by 8-keV electron interaction with the weld targets. As a final note, the Ukrainian scientists stated that "our military told us that it was safe." This investigation proved that operation of the ISWE could produce excessive radiation exposures, and proper shielding is required for prolonged operation.

This investigation produced an analytical method for predicting x-ray spectral and intensity distribution from electron impact targets. Verification of the method was obtained by comparing analytically predicted spectra to experimental spectra. This comparison shows that the analytical method is in agreement with experimental data.

The specific application of this analytical method was to calculate the biological-absorbed dose due to x rays transmitted through a variety of absorbers. Verification of this calculation was achieved by

normalizing the analytically generated x-ray spectrum to an equivalent exposure produced by operation of the ISWE electron beam welding tool and comparing calculated dose values to measured dose values. Measured dose values were obtained by exposing TLD's to x rays produced by operation of the ISWE electron beam welding tool. The normalizing factor for an equivalent ISWE electron beam welding tool exposure was the number of electrons incident on a metallic target. This value was calculated to be 8.55×10^{20} electrons. Calculation of this value is straightforward, given the electron beam current was 76 mA and the operation time was 1,800 sec (30 min). It should be noted that the value of 76 mA was provided by the Ukrainian scientists and not measured by NASA personnel.

Results of this comparison indicate that the analytical method of radiation dose calculation is equivalent, within calculated error, to the dose measured using the TLD's during an actual operation of the ISWE electron beam welding tool. Error calculations on the analytical and experimental data were performed using the technique of error propagation described by Bevington.[43]

7. SUMMARY

The objective of this investigation was to determine the absorbed radiation dose that an astronaut would receive while operating an electron beam welding system in the vacuum of space. The absorbed dose was initially measured using TLD's and subsequently verified using alternate experimental and analytical means. The goal of this investigation was to reduce the absorbed radiation dose an astronaut would receive to a value of 2 rem per 1,800-sec (30-min) operation of the ISWE electron beam welding system. This goal was achieved by incorporating a double layer of Teflon cloth on the exterior of the astronaut's space suit. This value of 2 rem per 1,800-sec (30-min) operation was verified by alternate experimental and analytical means. This investigation concentrated on a specific electron beam welding system that produced an electron beam of energy 8 keV with a beam current of 76 mA. The weld target used in this investigation was aluminum. The goal of this investigation was to reduce the absorbed dose for an astronaut operating this specific electron beam welding system and using aluminum as the weld metal.

The four experimental objectives were satisfactorily completed. The absorbed dose from x rays produced during operation of the ISWE electron beam welding tool was measured using TLD's. This measurement was the first known use of TLD's to measure absorbed dose from x rays of energy <10 keV.

A test system was developed using a low-current electron beam source that emulated the ISWE electron beam. This test system was used to generate experimental x-ray spectral data, which were subsequently used to verify an analytical approach to calculate x-ray spectral and intensity distributions. Various x-ray attenuating materials were studied in the test system, specifically to accumulate x-ray spectra of those x rays that were transmitted through the attenuating materials. These x-ray spectra of the transmitted x rays were also used to verify the analytical approach.

The objectives of the analytical portion of this investigation were satisfactorily completed. An analytical method was developed with a general expression that equates the x-ray intensity to experimental and geometry parameters. Solving this expression resulted in the generation of an x-ray spectrum that predicted the x-ray intensity to within a factor of 2 when compared to experimental data. This general expression for the x-ray spectral and intensity distribution was analytically propagated through various absorbers. The resulting attenuated x-ray spectrum intensity was within a factor of 2 when compared to experimental data. The attenuated x-ray spectrum was normalized to an equivalent ISWE exposure. Calculation of the absorbed dose, using this normalized x-ray spectrum, resulted in values that were within 20 percent of the measurements obtained using TLD's.

REFERENCES

1. Golightly, M.: Johnson Space Center, Private Communication, 1996.

2. Title 10, Chapter 20, Part 20 of the Code of Federal Regulations (10 CFR 20).

3. Protocol of Technological Apparatus Testing, UN 131.0100.000, Factory Number 01, Paton Welding Institute, Kiev, Ukraine, 1989.

4. Compton, A.H.; and Allison, S.K.: *X-Rays in Theory and Experiment*, 2nd ed., D. Van Nostrand Company, Princeton, New Jersey, p. 106, 1963.

5. Duane, W.; and Hunt, F.L.: "On X-Ray Wave-Lengths," *Proceedings of the American Physical Society*, Vol. 6, No. 2, pp. 166–171, 1915.

6. Dyson, N.A.: *X-Rays in Atomic and Nuclear Physics*, Longman Group Limited, London, England, p. 46, 1973.

7. Edwards, D.L.: "Test Report for the Assessment of Ground-Based Personnel and Crew Exposure to X-Ray Radiation During Electron Beam Welding Using the International Space Welding Experiment," p. AI–1, November 1996.

8. Lindhard, J.; Nielsen, V.; and Scharff, M.: "Approximation Method in Classical Scattering by Screened Coulomb Fields (Notes on Atomic Collisions, I)," *Det Kongelige Danske Videnskabernes Selskab Matemetisk-fysiske Meddelelser*, Vol. 36, No. 10, pp. 1–32, 1968.

9. Lindhard, J.; Scharff, M.; and Schiott, H.E.: "Range Concepts and Heavy Ion Ranges (Notes on Atomic Collisions, II)," *Det Kondelige Danske Videnskabernes Selskab Matemetisk-fysiske Meddelelser*, Vol. 33, No. 14, pp. 1–42, 1963.

10. Lindhard, J.; Nielsen, V.; Scharff, M.; and Thompson, P.V.: "Integral Equations Governing Radiation Effects (Notes on Atomic Collisions, III)," *Det Kongelige Danske Videnskabernes Selskab Matemetisk-fysiske Meddelelser*, Vol. 33, No. 10, pp. 1–40, 1963.

11. Seltzer, S.M.; and Berger, M.J.: "Bremsstrahlung Energy Spectra From Electrons with Kinetic Energy 1keV – 10 GeV Incident on Screened Nuclei and Orbital Electrons on Neutal Atoms with Z=1 – 100," *Atomic Data and Nuclear Data Tables*, Vol. 35, p. 345, 1986.

12. Seltzer, S.M.; and Berger, M.J.: "Bremsstrahlung Spectra From Electron Interactions with Screened Atomic Nuclei and Orbital Electrons," *Nuclear Instruments and Methods*, North-Holland, Amsterdam, B12, pp. 95–134, 1985.

13. Berger, M.J.; and Seltzer, S.M.: "Tables of Energy Losses and Ranges of Electrons and Positrons," *NASA SP–3012*, pp. 1–20, 1964.

14. Berger, M.J.; and Seltzer, S.M.: "Stopping Powers and Rangers of Electrons and Positrons," *NBSIR 82–2550*, pp. 1–28, 1982.

15. Bethe, H.; and Heitler, W.: "On the Stopping of Fast Particles and on the Creation of Positive Electrons," *Proceedings of the Royal Society*, London, Vol. A146, pp. 83–87, 1934.

16. Segrè, E.: *Experimental Nuclear Physics*, Vol. 1, John Wiley & Sons, Inc., New York, NY, p. 266, 1960.

17. Halbleib, J.A.; Kensek, R.P.; Mehlhorn, T.A.; Valdez, G.D.; Seltzer, S.M.; Berger, M.J.; "ITS Version 3.0: The Integrated TIGER Series of Coupled Electron/Photon Monte Carlo Transport Codes," *SAND91–1634* (March 1992).

18. Bertin, E.P.: *Principles and Practice of X-Ray Spectrometric Analysis*, Plenum Press, NY, p. 61, 1970.

19. Sulkanen, M.; Kolodziejczak, J.J.; and Chartas, G.; "Numerical Simulation of Electron-Impact X-ray Sources," *SPIE—The International Society for Optical Engineering—X-Ray and Extreme Ultraviolet Optics*, Vol. 2515, pp. 410–415, 1995.

20. Koch, H.W.; and Motz, J.W.: "Bremsstrahlun Cross-Section Formulas and Related Data," *Reviews of Modern Physics*, Vol. 31, No. 4, p. 931, October 1959.

21. Jackson, J.D.: *Classical Electrodynamics*, 2nd ed., John Wiley and Sons, New York, NY, p. 711, 1975.

22. Sulkanen, M.: *The XG Manual*, pp. 1–8, 1995.

23. Pella, P.A.; Feng, L.; and Small, J.A.: "An Analytical Algorithm for Calculation of Spectral Distributions of X-Ray Tubes for Quantitative X-Ray Fluorescence Analysis," *X-Ray Spectrometry*, Vol. 14, No. 3, pp. 125–135, 1985.

24. Gollnick, D.A.: *Basic Radiation Protection Technology*, 2nd ed., Pacific Radiation Corporation, Altadena, CA, pp. 67–103, 1989.

25. Henderson, B.J.: "Conversion of Neutron or Gamma Ray Flux to Absorbed Dose Rate," XDC 59–8–179, pp. 7–10, 1959.

26. Hubbell, J.H.: "Photon Cross Sections, Attenuation Coefficients, and Energy Absorption Coefficients From 10 keV to 100 GeV," *NSRDS–NBS 29*, pp. 1–77, 1969.

27. http://physics.nist.gov/PhysRefData/XrayMassCoef/ElemTab, September 7, 1998.

28. Fitzgerald, J.J.; Brownell, G.L.; and Mahoney, F.J.: *Mathematical Theory of Radiation Dosimetry*, Gordon and Breach Science Publishers, Inc., New York, NY, p. 265, 1967.

29. Schollhammer, F.R.: "Hand-Held Electron Beam Gun for In-Space Welding," Fourth Space Congress, Canaveral Council of Technical Societiewss, Session 15, pp. 1–31, April 1967.

30. Kuhar, M.: Victoreen, Private Communication, 1997.

31. Harris, W.; and Edwards, D.L.: "Evaluation of Exposure From a Low Energy X-Ray Device Using Thermoluminescent Dosimeters," *Proceedings of the 16th Annual Panasonic Dosimetry Symposium*, June 2–6, 1997.

32. Blackwood, O.H.; Osgood, T.H.; and Ruark, A.E.: *An Outline of Atomic Physics*, 3rd ed., John Wiley and Sons, New York, NY, p. 109, 1955.

33. Fuchs, E.; Oppolzer, H.; and Rehme, H.: *Particle Beam Microanalysis Fundamentals, Methods and Applications*, Verlagsgesellschaft mbH, Weinheim, Federal Republic of Germany pp. 227–273, 1990.

34. Van Grieken, R.E.; and Markowicz, A.A., Eds.: *Handbook of X-Ray Spectrometry Methods and Techniques*, Marcel and Dekker, Inc., New York, New York, 1993.

35. Azàroff, L.: *Elements of X-Ray Crystallography*, McGraw-Hill, New York, NY, pp. 96–108, 1968.

36. Bogdankevich, O.V.; and Nikolaev, F.A.: *Methods in Bremsstrahlung Research*, Academic Press, New York, NY, p. 2, 1966.

37. *Si(Li) Detector System Series 7300 Instruction Manual*, Canberra Industries, Meriden, CT, p. 10, 1992.

38. Grodstein, G.W.: *NBS Circular 583*, pp. 1–53, 1957.

39. Blatz, H., Editor-in-chief: *Radiation Hygiene Handbook*, 1st ed., McGraw-Hill, New York, NY, Chapter 14, p. 11, 1959.

40. Becker, K.: *Solid State Dosimetry*, CRC Press, Cleveland, OH, pp. 27–72, 1973.

41. Knoll, G.F.: *Radiation Detection and Measurement*, 2nd ed., John Wiley & Sons, New York, NY, pp. 444–465, 1989.

42. Weast, R.C., Ed.: *CRC Handbook of Chemistry and Physics*, 66th ed., CRC Press, Cleveland, OH, p. C–127, 1986.

43. Bevington, P.R.: *Data Reduction and Error Analysis for the Physical Sciences*, McGraw-Hill, New York, NY, pp. 56–58, 1969.

REPORT DOCUMENTATION PAGE

Form Approved
OMB No. 0704-0188

1. AGENCY USE ONLY *(Leave Blank)*	2. REPORT DATE	3. REPORT TYPE AND DATES COVERED
	November 2001	Technical Memorandum

4. TITLE AND SUBTITLE

Absorbed Dose Determination Using Experimental and Analytical Predictions of X-Ray Spectra

5. FUNDING NUMBERS

6. AUTHORS

D.L. Edwards

7. PERFORMING ORGANIZATION NAMES(S) AND ADDRESS(ES)

George C. Marshall Space Flight Center
Marshall Space Flight Center, AL 35812

8. PERFORMING ORGANIZATION REPORT NUMBER

M–1033

9. SPONSORING/MONITORING AGENCY NAME(S) AND ADDRESS(ES)

National Aeronautics and Space Administration
Washington, DC 20546–0001

10. SPONSORING/MONITORING AGENCY REPORT NUMBER

NASA/TM—2001–211383

11. SUPPLEMENTARY NOTES

Prepared by Materials, Processes, and Manufacturing, Engineering Directorate

12a. DISTRIBUTION/AVAILABILITY STATEMENT

Unclassified–Unlimited
Subject Category 99
Nonstandard Distribution

12b. DISTRIBUTION CODE

13. ABSTRACT *(Maximum 200 words)*

Electron beam welding in a vacuum is a technology that NASA is investigating as a joining technique for manufacture of space structures. This investigation characterizes the x-ray environment due to operation of an in-vacuum electron beam welding tool and provides recommendations for adequate shielding for astronauts performing the in-vacuum electron beam welding. NASA, in a joint venture with the Russian Space Agency, was scheduled to perform a series of welding in space experiments on board the U.S. Space Shuttle. This series of experiments was named the international space welding experiment (ISWE). The hardware associated with the ISWE was leased to NASA by the Paton Welding Institute (PWI) in Ukraine for ground-based welding experiments in preparation for flight. Two ground tests were scheduled, using the ISWE electron beam welding tool, to characterize the radiation exposure to an astronaut during the operation of the ISWE. These radiation exposure tests used thermoluminescence dosimeters (TLD's) shielded with material currently used by astronauts during extravehicular activities to measure the radiation dose. The TLD's were exposed to x-ray radiation generated by operation of the ISWE in-vacuum electron beam welding tool. This investigation was the first known application of TLD's to measure absorbed dose from x rays of energy <10 keV. The ISWE hardware was returned to Ukraine before the issue of adequate shielding for the astronauts was completely verified. Therefore, alternate experimental and analytical methods were developed to measure and predict the x-ray spectral and intensity distribution generated by ISWE electron beam impact with metal. These x-ray spectra were normalized to an equivalent ISWE exposure, then used to calculate the absorbed radiation dose to astronauts. These absorbed dose values were compared to TLD measurements obtained during actual operation of the ISWE in-vacuum electron beam welding tool. The calculated absorbed dose values were found to be in agreement with the measured TLD values.

14. SUBJECT TERMS

electron beam, welding, x ray, dosimeter, thermoluminescence

15. NUMBER OF PAGES

80

16. PRICE CODE

17. SECURITY CLASSIFICATION OF REPORT	18. SECURITY CLASSIFICATION OF THIS PAGE	19. SECURITY CLASSIFICATION OF ABSTRACT	20. LIMITATION OF ABSTRACT
Unclassified	Unclassified	Unclassified	Unlimited

National Aeronautics and
Space Administration
AD33
George C. Marshall Space Flight Center
Marshall Space Flight Center, Alabama
35812